

University of Alabama in Huntsville

**LOUIS**

---

Dissertations

UAH Electronic Theses and Dissertations

---

2021

## Unique approaches to novel antifungal discovery

Chelsea Nichole Powers

Follow this and additional works at: <https://louis.uah.edu/uah-dissertations>

---

### Recommended Citation

Powers, Chelsea Nichole, "Unique approaches to novel antifungal discovery" (2021). *Dissertations*. 391.  
<https://louis.uah.edu/uah-dissertations/391>

This Dissertation is brought to you for free and open access by the UAH Electronic Theses and Dissertations at LOUIS. It has been accepted for inclusion in Dissertations by an authorized administrator of LOUIS.

**UNIQUE APPROACHES TO NOVEL ANTIFUNGAL DISCOVERY**

by

**CHELSEA NICHOLE POWERS**

**A DISSERTATION**

**Submitted in partial fulfillment of the requirements  
for the degree of Doctor of Philosophy  
in  
The Biotechnology Science and Engineering Program  
to  
The School of Graduate Studies  
of  
The University of Alabama in Huntsville**

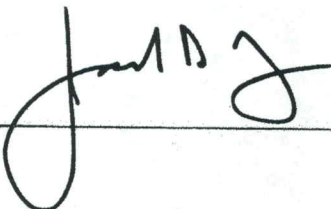
**HUNTSVILLE, ALABAMA**

**2021**


**DISSERTATION APPROVAL FORM**

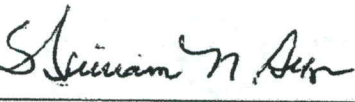
Submitted by Chelsea Nichole Powers in partial fulfillment of the requirements for the degree of Doctor of Philosophy in Biotechnology Science and Engineering and accepted on behalf of the Faculty of the School of Graduate Studies by the dissertation committee.

We, the undersigned members of the Graduate Faculty of The University of Alabama in Huntsville, certify that we have advised and/or supervised the candidate on the work described in this dissertation. We further certify that we have reviewed the dissertation manuscript and approve it in partial fulfillment of the requirements for the degree of Doctor of Philosophy in Biotechnology Science and Engineering.

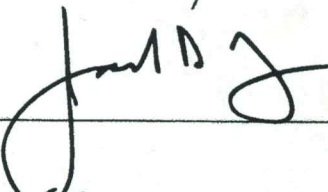
  
3/22/2021  
(Date) Committee Chair


  
3/20/2021

  
03/20/2021

  
3/21/21

 03/22/2021

  
3/22/2021 Department Chair

  
3/23/21 College Dean

*BA*

3/24/2021

Graduate Dean

---

<<<



## ACKNOWLEDGEMENTS

First and foremost, I would like to thank my academic advisor and sponsor, Dr. Robert McFeeters, for granting me permission to move forward with my project and his continuous advice, counseling, and support along the way. I will forever be grateful for the wisdom you have shared, the patience you have displayed, and the countless opportunities you have provided. Additionally, I would like to thank my committee members, Dr. William Setzer and Dr. Bernhard Vogler, for their direction and encouragement. Dr. Setzer kindly provided all of the plant extracts that were used for this research and provided me with guidance on how to carry forward with my project. Dr. Vogler spent countless hours teaching me various chemical instrumentation methods and frequently consulted with me on how to properly interpret data. I would also like to acknowledge Dr. John Mayo for working closely with me and providing invaluable microbiology instruction. I will always be extremely grateful for the time all of you invested in my education and for helping me learn how to be successful.

To my lab and office mates, each and every one of you has assisted and comforted me in a different way and I am forever happy that I got to spend this section of my life with you. I look forward to keeping in touch and I wish you all the very best.

I would like to thank the UAH Department of Chemistry for helping to fund my graduate education and research, and I would also like to directly thank Jeff Champoux for helping me with various academic issues along the way. Jeff, you are the best.

Lastly, I want to thank my friends and family for their continued love and support throughout my entire academic career. I want to specifically thank my mom for showing me daily how to have a good work ethic and for always reminding me how capable I am.

## TABLE OF CONTENTS

LIST OF FIGURES .....	ix
LIST OF TABLES.....	xii
CHAPTER 1: INTRODUCTION .....	1
1.1 <i>Cryptococcus neoformans</i> .....	1
1.2 Finding New Anticryptococcal Agents .....	3
1.3 Bioautography .....	4
CHAPTER 2: METHODS.....	6
2.1 Background.....	6
2.2 Bark Collection Location and Solvent Extraction .....	7
2.3 Microdilution Assay with Bark Extracts.....	10
2.4 Thin-Layer Chromatography .....	12
2.5 Agar-Overlay Bioautography.....	12
2.6 Preparative Thin-Layer Chromatography .....	13
2.7 Microdilution Assay with Prep-TLC Isolates.....	14
2.8 Nuclear Magnetic Resonance Spectroscopy .....	14
2.9 Gas Chromatography-Mass Spectrometry .....	15
CHAPTER 3: RESULTS AND DISCUSSION.....	16
3.1 Background.....	16
3.2 Microdilution Assay with Bark Extracts.....	16
3.3 Thin-Layer Chromatography Separation and Visualization .....	19

3.4 Bioautography .....	20
3.5 Microdilution Assay with Prep-TLC Isolates .....	23
3.6 Structure Determination for Prep-TLC Isolates.....	25
CHAPTER 4: CONCLUSIONS AND FUTURE WORK.....	38
4.1 Conclusions.....	38
4.2 Future Work.....	40
APPENDIX.....	42
REFERENCES .....	68



## LIST OF FIGURES

Figure		Page
3.2.1	Microdilution assay results from NPPEs 1-8 and the controls with <i>C. neoformans</i> (24067) in a 96-well plate.	17
3.2.2	Microdilution assay results from NPPEs 9-16 and the controls with <i>C. neoformans</i> (24067) in a 96-well plate.	18
3.4.1	Images of agar-overlay bioautography for NPPEs #7, #9, and #16 after staining with INT dye for 48 hours.	22
3.5	Microdilution assay results from the 8 prep-TLC isolates and the controls with <i>C. neoformans</i> (24067) in a 96-well plate.	23
3.6.1.A	The 500 MHz <sup>1</sup> H NMR spectrum for R <sub>f</sub> = 0.27 from extract #9 in CDCl <sub>3</sub> (7.26 ppm).	26
3.6.1.B	The 500 MHz <sup>1</sup> H NMR spectrum for R <sub>f</sub> = 0.51 from extract #9 in CDCl <sub>3</sub> (7.26 ppm).	27
3.6.1.C	The 500 MHz <sup>1</sup> H NMR spectrum for R <sub>f</sub> = 0.51 from extract #16 in CDCl <sub>3</sub> (7.26 ppm).	28
3.6.1.D	The 500 MHz <sup>1</sup> H NMR spectrum for R <sub>f</sub> = 0.58 from extract #16 in CDCl <sub>3</sub> (7.26 ppm).	29
3.6.2.A	Mass-to-charge ratio graph of R <sub>f</sub> = 0.27 from extract #9.	31
3.6.2.B	Mass-to-charge ratio graph of R <sub>f</sub> = 0.51 from extract #9.	32
3.6.2.C	Mass-to-charge ratio graph of R <sub>f</sub> = 0.51 from extract #16.	33
3.6.2.D	Mass-to-charge ratio graph of R <sub>f</sub> = 0.58 from extract #16.	34
3.6.3.A	Chemical structure of bornyl caffeate.	36
3.6.3.B	Chemical structure of bornyl ferulate.	37
A.1	Visualization of NPPE #1 after separation with 8:2 petroleum ether: ethyl acetate on a silica gel TLC plate.	43
A.2	Visualization of NPPE #2 after separation with 8:2 petroleum ether: ethyl acetate on a silica gel TLC plate.	44

A.3	Visualization of NPPE #4 after separation with 8:2 petroleum ether: ethyl acetate on a silica gel TLC plate.	45
A.4	Visualization of NPPE #5 after separation with 8:2 petroleum ether: ethyl acetate on a silica gel TLC plate.	46
A.5	Visualization of NPPE #6 after separation with 8:2 petroleum ether: ethyl acetate on a silica gel TLC plate	47
A.6	Visualization of NPPE #7 after separation with 8:2 petroleum ether: ethyl acetate on a silica gel TLC plate.	48
A.7	Visualization of NPPE #8 after separation with 8:2 petroleum ether: ethyl acetate on a silica gel TLC plate.	49
A.8	Visualization of NPPE #9 after separation with 8:2 petroleum ether: ethyl acetate on a silica gel TLC plate.	50
A.9	Visualization of NPPE #11 after separation with 8:2 petroleum ether: ethyl acetate on a silica gel TLC plate.	51
A.10	Visualization of NPPE #13 after separation with 8:2 petroleum ether: ethyl acetate on a silica gel TLC plate.	52
A.11	Visualization of NPPE #14 after separation with 8:2 petroleum ether: ethyl acetate on a silica gel TLC plate.	53
A.12	Visualization of NPPE #16 after separation with 8:2 petroleum ether: ethyl acetate on a silica gel TLC plate.	54
A.13	Visualization of NPPE #7 after separation with 7:3 petroleum ether: ethyl acetate on a silica gel TLC plate.	55
A.14	Visualization of NPPE #9 after separation with 7:3 petroleum ether: ethyl acetate on a silica gel TLC plate.	56
A.15	Visualization of NPPE #16 after separation with 7:3 petroleum ether: ethyl acetate on a silica gel TLC plate.	57
A.16	Images of agar-overlay bioautography for NPPEs #1, #2, and #4 after staining with INT dye for 48 hours.	58
A.17	Images of agar-overlay bioautography for NPPEs #5, #6 and #8 after staining with INT dye for 48 hours.	59
A.18	Images of agar-overlay bioautography for NPPEs #11, #13, and #14 after staining with INT dye for 48 hours.	60

A.19	Images of agar-overlay bioautography for NPPEs #7, #9, and #16 after staining with INT dye for 48 hours.	61
A.20	Heteronuclear single quantum correlation (HSQC) spectrum of prep-TLC isolate #3 (NPPE #9, $R_f = 0.25$ ).	62
A.21	Heteronuclear multiple bond correlation (HMBC) spectrum of prep-TLC isolate #3 (NPPE #9, $R_f = 0.25$ ).	63
A.22	$^1\text{H}$ - $^1\text{H}$ correlation (COSY) spectrum of prep-TLC isolate #3 (NPPE #9, $R_f = 0.25$ ).	64
A.23	Heteronuclear single quantum correlation (HSQC) spectrum of prep-TLC isolate #4 (NPPE #9, $R_f = 0.51$ ).	65
A.24	Heteronuclear multiple bond correlation (HMBC) spectrum of prep-TLC isolate #4 (NPPE #9, $R_f = 0.51$ ).	66
A.25	$^1\text{H}$ - $^1\text{H}$ correlation (COSY) spectrum of prep-TLC isolate #4 (NPPE #9, $R_f = 0.51$ ).	67

## LIST OF TABLES

Table		Page
3.2	Results from the microdilution assay for NPPEs from Monteverde, Costa Rica against <i>Cryptococcus neoformans</i> (24067).	19
3.5	Results from the microdilution assay for prep-TLC isolates against <i>Cryptococcus neoformans</i> (24067).	24
3.6.2	Summary of the GC-MS results for the 4 prep-TLC isolates.	35
3.6.3.A	NMR assignments for $R_f = 0.27$ from extract #9.	36
3.6.3.B	NMR assignments for $R_f = 0.51$ from extract #9.	37
A.1	Combined information regarding the NPPEs used for this Thesis.	42

## CHAPTER ONE

### INTRODUCTION

#### 1.1 *Cryptococcus neoformans*

It is estimated that 1.5 million people die each year from fungal infections primarily caused by three distinct fungal species, one being *Cryptococcus*, which alone infects over 1 million people (Revie et al. 2018; Xie et al. 2014). *Cryptococcus neoformans* is a basidiomycete fungus that is a well-known opportunistic human and animal pathogen. It is commonly found throughout most environments, particularly prominent in bird droppings, soil, and decaying wood (Domaneschi et al. 2018; Montagna et al. 2018; Polvi et al. 2015). The ability to grow at 37 °C, a polysaccharide capsule, and melanin formation allow *C. neoformans* to not only survive, but thrive in the human body (Desjardins et al. 2017). In 2009, approximately 65% of HIV/AIDS patients that acquired cryptococcal meningitis died as a result of the infection (Park et al. 2009). However recent global analysis determined that approximately 82% of HIV/AIDS patients that acquired cryptococcal meningitis died as a result of the infection, and that cryptococcal meningitis is responsible for approximately 15% of HIV/AIDS-related deaths (Rajasingham et al. 2017).

As recommended by the Centers for Disease Control, the Infectious Diseases Society of America, and the World Health Organization, the main treatment options for

cryptococcal infections are fluconazole, amphotericin B, and flucytosine. This antifungal trio is expensive, averaging about \$31,000 per patient (Jung et al. 2018). Along with the high price tag comes an even higher risk for severe, unwanted side effects. As listed by the American Society of Health-System Pharmacists, the side effects of this antifungal trio range from moderate effects including vomiting, rashes, diarrhea, loss of appetite, and headaches, to severe and deadly side effects such as hypotension, seizures, psychosis, organ damage, and organ failure. Even with these treatment options, excluding the potential side effects, there is still a high percentage of mortality during the course of cryptococcal meningitis treatment (Hardison and Brown 2012). This means there is a chance that the current antifungal regimen for *C. neoformans* infections will fail, highly depending on the patient, the strain, and the duration of infection before diagnosis. All things considered, the need for new anticryptococcal treatments is dire.

With the lack of new antifungal drug development, current clinically prescribed antifungals are losing their efficacy. Since *C. neoformans* exhibits high genomic plasticity, the expression of azole-based antifungal targets is likely to quickly change, leading to azole resistance (Perlin, Rautemaa-Richardson, and Alastruey-Izquierdo 2017; Revie et al. 2018). This reduces the potency of one of the recommended treatment options, fluconazole. Also, almost two decades ago, there were reports that another recommended treatment option, Amphotericin B, failed for *C. neoformans* infection (Perfect and Cox 1999). While still largely uncommon, strains of the fungus continue to be isolated from patients showing resistance to or reduced effectiveness from treatment with Amphotericin B (Xie et al. 2014). Resistance to the last of the mentioned antifungal trio, flucytosine, is quite common, and is why the drug is mostly used as an adjunctive instead as a primary treatment option (Campoy and Adrio 2017; Xie et al. 2014).

## 1.2 Finding New Anticryptococcal Agents

Humans have used medicines derived from plants to treat a range of ailments for centuries, dating back as far as 2600 B.C (Gurnani et al. 2014). From the approximated 250,000 natural products with currently known biological activity, 60% were isolated from plant species (Demain 2014). Natural product plant extracts (NPPEs) are remarkably diverse due to the complexity of their unique compositions, and because they are also renewable resources, they pose to be excellent sources for drug discovery (Balouiri, Sadiki, and Ibnsouda 2016; Abad 2006). There is already an enormous standing market for plant-based medicines sold under the more common term, herbal supplements. The total estimated retail sales of herbal supplements derived from plants in the United States alone in 2016 was \$7.5 billion, a \$3.3 billion increase from 2000 (estimated at \$4.2 billion), and \$2.4 billion increase from 2010 (estimated at \$5.0 billion) (Smith et al. 2017). In the past 30 years new drugs derived from a natural product extract have been approved for treating numerous illnesses (analgesic, antimicrobial, contraception, hemostatic, immunosuppressant, neuroleptic, osteoporosis, vasodilation, etc.) (Newman and Cragg 2016). However, with all the medical success of finding new plant-based treatment options for various ailments, new therapies for cryptococcal infection have not been extensively investigated. Accordingly, it has been over 25 years since new therapeutic options for *Cryptococcus* infection have been developed (Perfect 2017).

All of the NPPEs used in this study were collected from Monteverde, Costa Rica. The search for new anticryptococcal agents began here because the area is extremely biodiverse, which increases the chance of finding plant species containing new treatment options for cryptococcal infection. Furthering our interests was the fact that there have

already been several studies published claiming the antifungal activity of plant extracts from Costa Rica (Ficker et al. 2003; Prieto et al. 2011; DeMera and Angert 2004; Amiguet et al. 2006; Svetaz et al. 2010). It was our belief that if plant extracts from this region already showed potent antifungal activity, some extracts would reveal to be anticryptococcal agents as well.

### **1.3 Bioautography**

Once a NPPE has been identified to have strong anticryptococcal activity, it is important to determine exactly which component(s) are responsible for the activity. A quick, inexpensive, and effective technique for detecting biologically active components in NPPEs is bioautography (Dewanjee et al. 2015; Guerrini et al. 2016; Favre-Godal, Queiroz, and Wolfender 2013). This technique is a bioassay and provides experimental evidence as to whether or not a compound will affect the growth of a microorganism. There are generally three main accepted procedural types of bioautography: (1) agar diffusion, (2) direct, and (3) agar-overlay (Balouiri, Sadiki, and Ibnsouda 2016; Marston 2011). For all of the procedures, the extract of interest must first be separated using TLC. The difference between the procedures exists largely with how the microbial species are grown, either (1) diffusing the spots from the TLC plate onto an agar medium containing the species, (2) dipping the TLC plate into a media suspension with the species, or (3) pouring an agar-broth solution of the species on top of the TLC plate. Microbes are grown until zones of inhibition can be visualized. Specifically with *C. neoformans*, bioautography has been shown to work well using the agar-overlay method with a dye for easy visualization and determination of active anticryptococcal components (Fabri et al. 2011; Fernández et al. 2014; Tavares et al. 2014). After zones of inhibition are



visualized, prep-TLC may be performed to isolate zones of inhibition based on the calculated retention factor ( $R_f$ ) values. Furthermore, once the active components of an extract have been isolated using prep-TLC, the isolates can be analyzed and identified using analytical techniques, such as NMR spectroscopy, GC, liquid chromatography (LC), and MS.

The focus of this work was to isolate and identify the active anticryptococcal components of new NPPEs from Costa Rica. Agar-overlay bioautography in combination with a tetrazolium dye was used to visualize the active components, while prep-TLC was used to isolate the components. The isolated components were retested for anticryptococcal activity and once activity was confirmed, an attempt was made at identification using NMR and GC-MS.

## CHAPTER TWO

### METHODS

#### 2.1 Background

Plant extracts are unique and inexpensive sources that are hosts to many different small molecules. Potentially, these small molecules could be biologically active, offering new therapeutic options for a range of illnesses. Thus, it is important to evaluate plant extracts and identify any new sources of medically relevant compounds. This work specifically focuses on finding new compounds from bark extracts that inhibit the growth of the pathogenic fungus *C. neoformans*. Microdilution assays were performed first to determine whether the extracts had any initial activity against *C. neoformans*.

Bioautography with the fungus and the extracts was used to locate inhibition zones on TLC plates. For any inhibition zone, a  $R_f$  value was calculated in order to identify the zone later when performing prep-TLC. Prep-TLC was incorporated to purify out the active component from the rest of the extract. Once separated, prep-TLC isolates were subjected to analytical techniques in an attempt to identify the component(s).

## **2.2 Bark Collection Location and Solvent Extraction**

All natural product extracts were kindly provided by Dr. William N. Setzer and the UAH Natural Product Drug Discovery Group (NPDDG).

### **2.2.1 *Machaerium biovalatum* (#1)**

Bark was collected on the 16<sup>th</sup> of May in 2001 between Santa Elena and San Luis, Monteverde, Costa Rica (10° 15.5' N, 84° 50.3' W, 879 m above sea level (asl)). Extract was collected by Soxhlet extraction. The dried bark was refluxed with acetone 6 hours.

### **2.2.2 *Ocotea* sp. “los llanos” (#2)**

Bark was collected on the 19<sup>th</sup> of May in 2006 from Los Llanos, Monteverde, Costa Rica (10° 18' 18.4" N, 84° 50' 9.1" W, 1254 m asl). Extract was collected by Soxhlet extraction. The dried bark was refluxed with acetone for 6 hours.

### **2.2.3 *Diospyros digyna* (#3)**

Bark was collected on the 28<sup>th</sup> of May in 2006 from San Luis, Monteverde, Costa Rica (10° 16.6' N, 84° 48.5' W, 882 m asl). Extract was collected by Soxhlet extraction. The dried bark was refluxed with ethanol for 6 hours.

### **2.2.4 *Psychotria parvifolia* (#4)**

Bark was collected on the 19<sup>th</sup> of May in 1999 from the Monteverde Cloud Forest Preserve in Monteverde, Costa Rica (10° 20.9' N, 84° 45.8' W, 1530 m asl). Extract was collected by Soxhlet extraction. The dried bark was refluxed with acetone for 6 hours (M. C. Setzer et al. 2003).

### **2.2.5 *Cedrela tonduzii* (#5)**

Bark was collected on the 18<sup>th</sup> of May in 2007 from Productores de Monteverde in Monteverde, Costa Rica (10° 18.7' N, 84° 48.6' W, 1350 m asl). Extract was collected by Soxhlet extraction. The dried bark was refluxed with acetone for 6 hours (Eason and Setzer 2007).

### **2.2.6 *Lonchocarpus oliganthus* (#6)**

Bark was collected on the 16<sup>th</sup> of May in 2008 from Monteverde, Costa Rica (10° 19' 3.57" N, 84° 47' 38.03" W, 1459 m asl). Extract was collected by Soxhlet extraction. The dried bark was refluxed with acetone for 6 hours (Deskins et al. 2014).

### **2.2.7 *Croton monteverdensis* (#7)**

Bark was collected on the 22<sup>nd</sup> of May in 2001 from Hotel El Bosque in Monteverde, Costa Rica (10° 18.7' N, 84° 48.6' W, 1325 m asl). Extract was collected by Soxhlet extraction. The dried bark was refluxed with dichloromethane for 6 hours (W. N. Setzer 2006).

### **2.2.8 *Tapirira mexicana* (#8)**

Bark was collected on the 19<sup>th</sup> of May in 1998 from Hotel El Bosque in Monteverde, Costa Rica (10° 18.7' N, 84° 48.6' W, 1325 m asl). Extract was collected by Soxhlet extraction. The dried bark was refluxed with ethanol for 6 hours (M. C. Setzer et al. 2003).

### **2.2.9 *Verbesina turbacensis* (#9)**

Bark was collected on the 5<sup>th</sup> of May in 2008 from the San Luis Biological Station in Monteverde, Costa Rica (10° 15' 49" N, 84° 49' 52" W, 700 m asl). Extract was collected by Soxhlet extraction. The dried bark was refluxed with acetone for 6 hours (Ogungbe et al. 2010).

### **2.2.10 *Styphnolobium monteviridis* (#10)**

Bark was collected on the 3<sup>rd</sup> of June in 2004 from Hotel El Bosque in Monteverde, Costa Rica (10° 18.7' N, 84° 48.6' W, 1350 m asl). Extract was collected using Soxhlet extraction. The dried bark was refluxed with chloroform for 6 hours.

### **2.2.11 *Myrcianthes* sp. "black fruit" (#11)**

Bark was collected on the 14<sup>th</sup> of May in 1997 from Hotel El Bosque in Monteverde, Costa Rica (10° 18.7' N, 84° 48.6' W, 1350 m asl). Extract was collected using Soxhlet extraction. The dried bark was refluxed with dichloromethane for 6 hours (M. C. Setzer et al. 2003).

### **2.2.12 *Cupania glabra* (#12)**

Bark was collected on the 5<sup>th</sup> of May in 2002 from Hotel El Bosque in Monteverde, Costa Rica (10° 18.7' N, 84° 48.6' W, 1350 m asl). Extract was collected using Soxhlet extraction. The dried bark was refluxed with dichloromethane for 6 hours (W. N. Setzer et al. 2005).

### **2.2.13 *Ardisia revoluta* (#13)**

Bark was collected on the 24<sup>th</sup> of May in 2000 from the San Luis Biological Station in Monteverde, Costa Rica (10° 15' 49" N, 84° 49' 52" W, 700 m asl). Extract was collected using Soxhlet extraction. The dried bark was refluxed with acetone for 6 hours.

### **2.2.14 *Erythrina lanceolata* (#14)**

Bark was collected on the 5<sup>th</sup> of May in 2007 from Hotel El Bosque in Monteverde, Costa Rica (10° 18.7' N, 84° 48.6' W, 1350 m asl). Extract was collected using Soxhlet extraction. The dried bark was refluxed with dichloromethane for 6 hours.

### **2.2.15 *Bursera ovalifolia* (#15)**

Bark was collected on the 14<sup>th</sup> of May in 2008 from Monteverde, Costa Rica (10° 17' 5.5" N, 84° 48' 27.7" W, 1042 m asl). Extract was collected using Soxhlet extraction. The dried bark was refluxed with chloroform for 6 hours.

### **2.2.16 *Bocconia frutescens* (#16)**

Bark was collected on the 8<sup>th</sup> of June in 2004 from Monteverde, Costa Rica (10° 18' 50.1" N, 84° 48' 47.5" W, 1388 m asl). Extract was collected using Soxhlet extraction. The dried bark was refluxed with acetone for six hours.

## **2.3 Microdilution Assay with Bark Extracts**

All extracts were diluted in dimethyl sulfoxide at concentrations of 0.01 mg/mL (1%) and stored in a refrigerator at 4 °C. *Cryptococcus neoformans* (ATCC 24067) was grown in potato dextrose broth (PDB, Difco by Becton, Dickinson and Company) at

37 °C for three days in a shaking incubator. An isolation streak was performed with the broth solution of the fungus on potato dextrose agar (PDA, Difco by Becton, Dickinson and Company) plates and grown at 37 °C for three days. From this, a single colony was selected and grown again in PDB for three days in a shaking incubator. From the second broth solution, 2 µL of cells were aliquoted into 200 mL of fresh PDB, of which 10 µL was added to a hemacytometer (Bright-Line, Hausser Scientific) and counted. After cell calculations, the cells were subsequently diluted to  $2.0 \times 10^3$  cells/mL in RPMI 1640 (Roswell Park Memorial Institute, Mediatech, Inc.) buffered with 167 mM MOPS (3-(N-morpholino)propanesulfonic acid) at pH 7.0.

The 96-well plate microdilution method was used. To begin, 100 µL of RPMI/MOPS was added to every well in the 96-well plate (sterile polystyrene U-bottom with low evaporation lid, Corning). Then 100 µL of the natural product extracts along with DMSO as a solvent control and 100 µM Amphotericin B (AmpB, from *Streptomyces nodosus*, Alfa Aesar) as a positive control were added to the first row of each column and serially diluted by two-fold down the column. The solvent control was included to distinguish between growth inhibition from the solvent versus inhibition from the extracts. The positive control was included to visualize complete inhibition and in order to compare inhibition between that of a known antifungal and the extracts. A negative control of RPMI alone was also included to ensure cell growth was normal. Finally, 100 µL of fungal cells at a concentration of  $2.0 \times 10^3$  cells/mL were added to every well in the plate. Plates were incubated at 37 °C for three days. Fungal inhibition was interpreted visually through comparison to the positive and negative controls using a Darkfield Quebec Colony Counter (American Optical Company). Samples were screened in triplicate.

## 2.4 Thin-Layer Chromatography

Extracts #3, 10, 12, and 15 were not used for this assay due to lack of supply. The remaining extracts were diluted in acetone at concentrations of 10 mg/mL and stored in a refrigerator at 4 °C.

Each extract, in 5 µL volumes, was run on 200 µm silica TLC plates (Silica G TLC plates with UV 254, Sorbtech) using a solvent system of petroleum ether and ethyl acetate at a ratio of 8:2. If this solvent system did not provide adequate separation, a ratio of 7:3 petroleum ether and ethyl acetate was used instead.

To visualize plates, they were first subjected to short wave UV light using a MINERALIGHT® UVS-254 lamp. Plates were then placed in iodine chambers for 10 minutes. The chambers consisted of iodine crystals in dark amber glass jars.

## 2.5 Agar-Overlay Bioautography

*C. neoformans* cells were grown as described above in Methods 2.3 and diluted to a concentration  $1.0 \times 10^6$  cells/mL. NPPEs were run on TLC plates before use in the bioautography assay. They were run approximately two hours before and kept in a sterile plastic container to allow solvent evaporation and reduce contamination. These plates were subjected to UV light to confirm the extract ran in a straight line, however plates were not subjected to iodine chambers. To glass test tubes (borosilicate 18 x 150 mm disposable culture tubes) in a water bath at 45 °C, 6 mL of Mueller-Hinton broth:agar (MHB, Difco by Becton, Dickinson and Company; laboratory grade agar from Fisher Scientific) at a ratio of 8:2 was added. The bath was turned off, allowing the broth:agar solution to cool. At 39 °C, fungal cells were added to the broth:agar solution to a final concentration of  $1.0 \times 10^6$  cells/mL. Cells must be added at this temperature because this



is the maximum temperature for *C. neoformans* cell growth (Madeira-Lopes, Plácido, and Cabeça-Silva 1986) and because below this temperature the agar begins to solidify. Cells were immediately poured over the pre-run TLC plates inside of a sterile plastic container. Plates were allowed to solidify before adding small pieces of damp, sterile paper towels on the opposite side of the container. Containers were then placed inside an incubator at 37 °C. After 24 hours, containers were removed and the plates were sprayed with 2.5 mg/mL 2-(4-iodophenyl)-3-(4-nitrophenyl)-5-phenyltetrazolium chloride dye (INT, Tokyo Chemical Industry Co., Ltd), and incubated again at 37 °C. After 4, 24, and 48 hours of further incubation, plates were visually evaluated for zones of inhibition.  $R_f$  values of the zones of inhibition were calculated using Equation 1 listed below.

Additionally, once zones of inhibition had been identified using regular TLC plates, the procedure was repeated on the prep-TLC plates to be used for inhibition zone isolation. This was done to ensure that  $R_f$  values were the same. Prep-TLC plates (Fluka Analytical®) were silica gel-based with a glass back, a fluorescent indicator, and a 60 Å medium pore diameter. Plates were cut into L x W 10 cm x 4 cm rectangles using a glasscutter before use. Extracts were run on the prep-TLC plates like the regular TLC plates, as described above in Methods 2.4.

Equation 1: 
$$R_f = \frac{\text{Distance spot traveled in solvent system}}{\text{Distance solvent front traveled}}$$

## 2.6 Preparative Thin-Layer Chromatography

Extracts were separated in a solvent system of petroleum ether and ethyl acetate in a ratio of 7:3 on prep-TLC plates as described above in Methods 2.4 and 2.5. Prep-TLC plates for this procedure were cut into L x W 10 cm x 10 cm rectangles. Dried

extract was mixed with acetone or dichloromethane and added to the bottom of the prep-TLC plates 1.5 cm above the edge of the plate in a thick, straight line. After running the plates, the bands that showed activity from the agar-overlay bioautography with the prep-TLC plates were carefully scraped out with a metal scoopula based on their calculated  $R_f$  values. The powder was then added to a glass vial and dissolved overnight at room temperature in chloroform. Following, the solution was filtered through Q5 filter paper (medium flow rate and porosity) into a new glass vial. The vial was left uncapped in a hood overnight to evaporate off the solvent.

### **2.7 Microdilution Assay with Prep-TLC Isolates**

Prep-TLC isolates were subjected to the microdilution assay as performed above in Methods 2.3 with the whole bark extracts and *C. neoformans* (24067). The isolates were diluted to a concentration of 10 mg/mL in DMSO for use in the assay. The same controls that were used to evaluate the whole bark extracts were used again: DMSO, 100  $\mu$ M AmpB, and a negative control of RPMI alone. The assay was also performed in triplicate.

### **2.8 Nuclear Magnetic Resonance Spectroscopy**

A 500 MHz Varian Unity Inova spectrometer was used to collect all of the data at room temperature (25 °C). This spectrometer was equipped with a 5-mm triple resonance inverse detectable probe. All of the prep-TLC isolates subjected to NMR spectroscopy were dissolved in deuterated chloroform (Cambridge Isotope Laboratories, Inc.) to an approximate concentration of 5 mg/mL. Proton ( $^1\text{H}$ ), heteronuclear single quantum

correlation (HSQC), heteronuclear multiple bond correlation (HMBC), and  $^1\text{H}$ - $^1\text{H}$  correlation (COSY) spectra were acquired for all samples.

## **2.9 Gas Chromatography-Mass Spectrometry**

Analysis of the prep-TLC isolates was completed using an Agilent 6890 Series GC system with an Agilent 5973 Network Mass Selective Detector. The system was equipped with an Agilent HP-5MS capillary column (length 30 m, diameter 0.250 mm, and film thickness 0.25  $\mu\text{M}$ ). The carrier gas was helium, with a flow rate of 1.5 mL/minute. Column temperature was initially 60  $^{\circ}\text{C}$ , and gradually increased to 310  $^{\circ}\text{C}$  at a rate of 6  $^{\circ}\text{C}$  per minute. A solvent delay of 3.5 minutes was used. Each sample was dissolved in chloroform at a concentration of 1 mg/mL. Samples were injected in 1.0  $\mu\text{L}$  volumes using an Agilent 7693 Autosampler in splitless mode.

## CHAPTER 3

### RESULTS AND DISCUSSION

#### 3.1 Background

This study began by evaluating anticryptococcal activity via broth microdilution of 16 NPPEs from Monteverde, Costa Rica. The extracts were then subjected to agar-overlay bioautography to visualize zones of inhibition. Extracts that showed zones of inhibition were further evaluated by purifying out the active components using prep-TLC. Prep-TLC isolates were screened for anticryptococcal activity using broth microdilution. If the prep-TLC isolates showed anticryptococcal activity, an attempt was made to identify the compound(s) using chemical instrumentation methods.

#### 3.2 Microdilution Assay with Bark Extracts

MIC values of the 16 NPPEs were measured using a 96-well plate microdilution assay in triplicate. This assay was performed to determine whether the full NPPE would inhibit the growth of *C. neoformans* (24067). The solvent control, pure DMSO, inhibited *C. neoformans* at 6.25%, while the positive control, 100  $\mu$ M AmpB, inhibited the fungus at a concentration of 1  $\mu$ M. The RPMI media control exhibited normal growth in all wells. Images of the 96-well plates are shown in Figures 3.2.1 and 3.2.2. The MIC values for the NPPEs with *C. neoformans* (24067) are listed in Table 3.2.

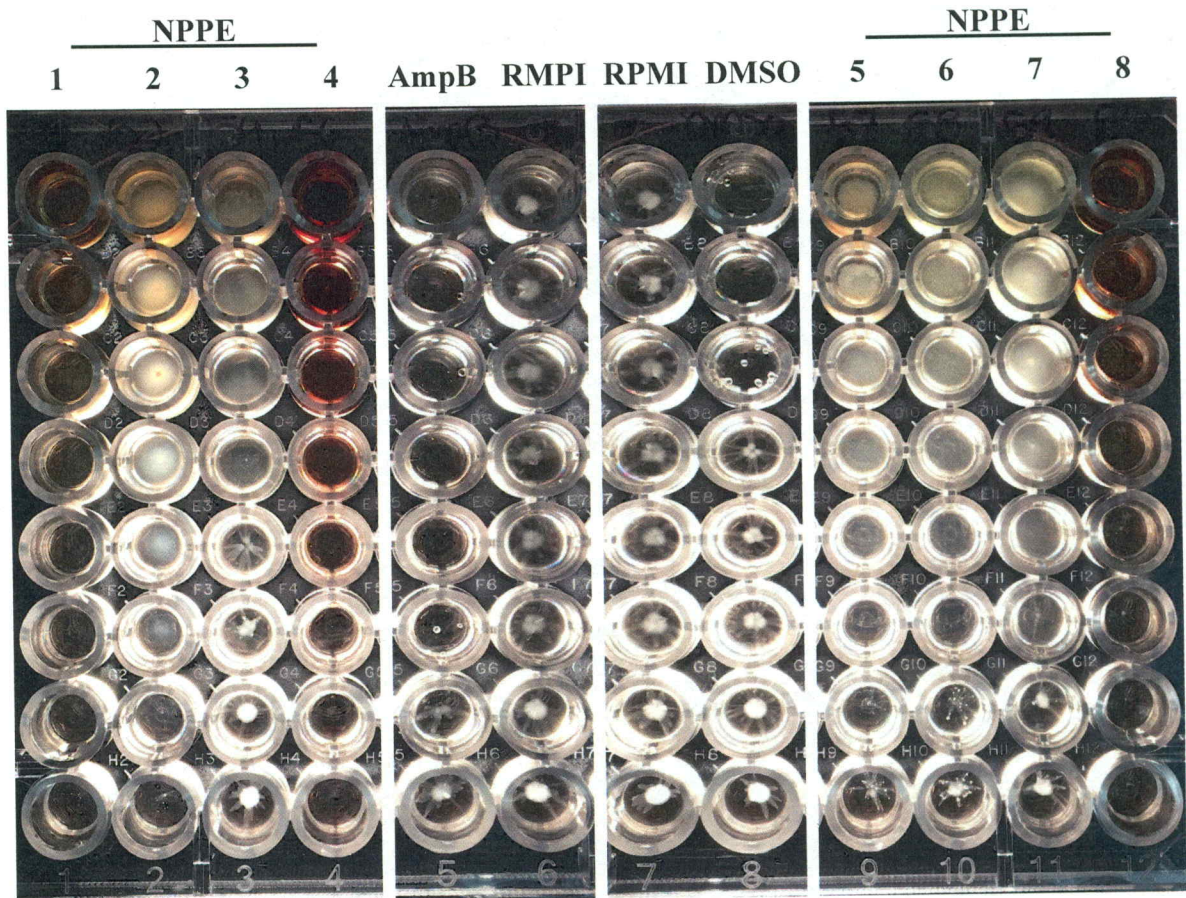


**Figure 3.2.1** Microdilution assay results from NPPEs 1-8 and the controls with *C. neoformans* (24067) in a 96-well plate. Both RPMI media controls containing only cells grew, showing that cells were healthy. Samples and controls were added to the first row in each column and serially diluted down the column. The photo of the plate was divided into sections to emphasize the difference between the results from the controls versus the results from the extracts. The small, white clumps in the middle of each well are growth of *C. neoformans*. The fluffy, grainy, or cloudy appearances in some of the wells are insoluble solids from the NPPEs.

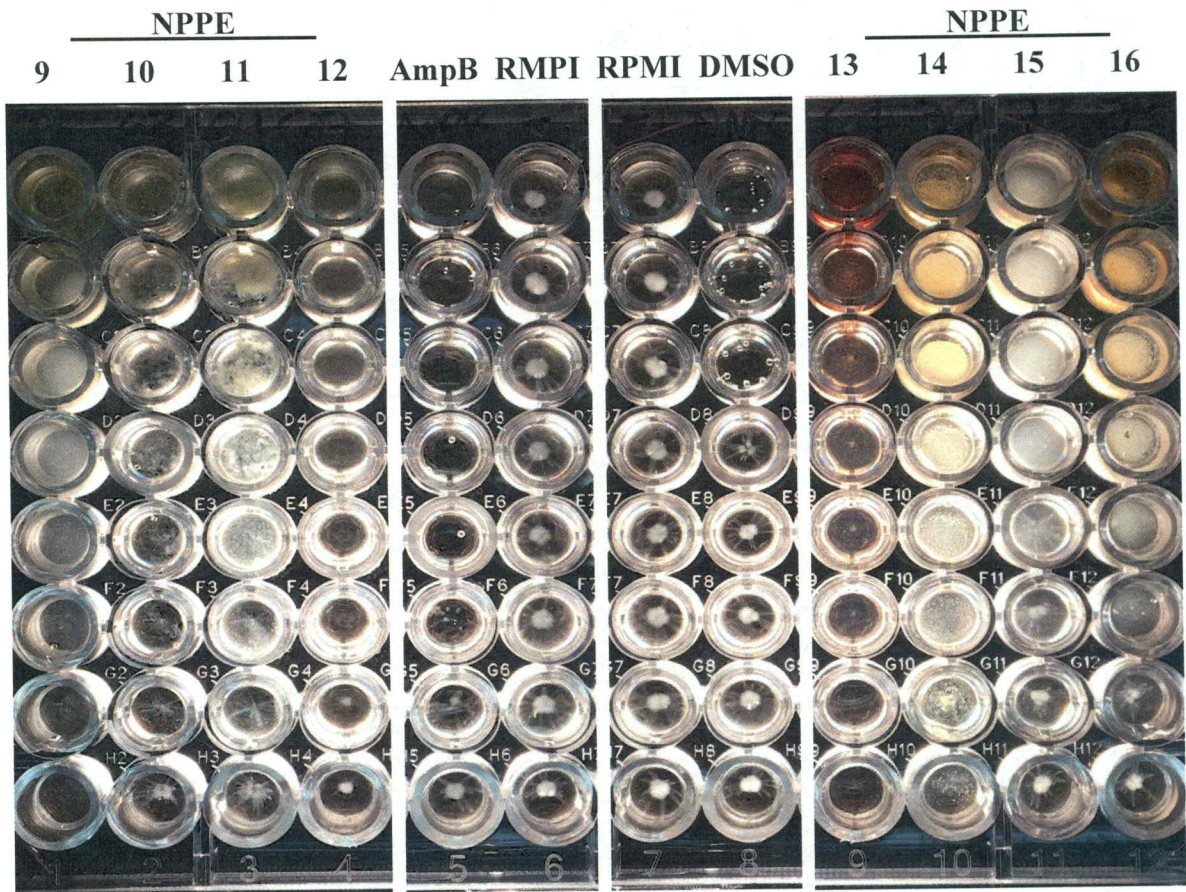


**Figure 3.2.2** Microdilution assay results from NPPEs 9-16 and the controls with *C. neoformans* (24067) in a 96-well plate. Both RPMI media controls containing only cells grew, showing that cells were healthy. All samples and controls were added to the first row in each column and serially diluted down the column. The photo of the plate was divided up into sections to emphasize the difference between the results from the controls versus the results from the extracts. The small, white clumps in the middle of each well are growth of *C. neoformans*. The fluffy, grainy, or cloudy appearances in some of the wells are insoluble solids from the NPPEs.

**Table 3.2** Results from the microdilution assay for NPPEs from Monteverde, Costa Rica against *C. neoformans* (24067). The observed MIC value in parts per million is shown in the right column. Results were interpreted visually from the 96-well MIC plates based on growth of the fungus.

NPPE Number	Plant Name	MIC (ppm)
1	<i>Machaerium biovalatum</i>	20
2	<i>Ocotea</i> sp. “los llanos”	20
3	<i>Diospyros digyna</i>	315
4	<i>Psychotria parvifolia</i>	20
5	<i>Cedrela tonduzii</i>	80
6	<i>Lonchocarpus oliganthus</i>	80
7	<i>Croton monteverdensis</i>	155
8	<i>Tapirira mexicana</i>	20
9	<i>Verbesina turbacensis</i>	20
10	<i>Styphnolobium monteviridis</i>	80
11	<i>Myrcianthes</i> sp. “black fruit”	155
12	<i>Cupania glabra</i>	80
13	<i>Ardisia revoluta</i>	20
14	<i>Erythrina lanceolata</i>	20
15	<i>Bursera ovalifolia</i>	315
16	<i>Bocconia frutescens</i>	80

### 3.3 Thin-Layer Chromatography Separation and Visualization

TLC was performed in order to separate the components of the NPPEs. UV fluorescent-imbedded silica gel-based TLC plates were used as the stationary phase, while both UV light and iodine chamber exposures were used to visualize the separations. The mobile/gas phase consisted of petroleum ether (PetEt), which is a nonpolar solvent, and ethyl acetate (EtOAc), which is polar. A mixture in a ratio of 8:2 PetEt:EtOAc was used as a starting point. All 12 NPPEs were subjected to TLC via these conditions.

Additionally, 3 of the NPPEs (#7, #9, and #16) were subjected to TLC but with a solvent system of 7:3 PetEt:EtOAc after it was noted in the first bioautographic analysis (explained in Results Section 3.4) that the components could be further separated. Images of NPPEs after separation with 8:2 PetEt:EtOAc and visualization both under a UV lamp and after a 10-minute exposure to an iodine chamber can be seen in the Appendix, Figures 1-12. The 3 NPPEs (#7, #9, and #16) after separation with 7:3 PetEt:EtOAc and visualization can be seen in the Appendix, Figures 13-15. Other solvent systems, such as PetEt:EtOAc in a ratio of 6:4, and PetEt:EtOAc:Methanol in ratios of 7:2:1 and 6:3:1, were also tested but decreased separation of spots for these 3 NPPEs (data not shown).

### **3.4 Bioautography**

Agar-overlay bioautography was performed after separating the NPPEs in a solvent system of PetEt:EtOAc in a ratio of 8:2. From the 12 NPPEs evaluated using this procedure, 6 showed no zones of inhibition (#1, #5, #6, #8, #11, #14), 3 showed inhibition only over the original spot on the TLC plate (#2, #4, #13), and 3 showed multiple zones with different  $R_f$  values (#7, #9, and #16). The results from the 9 NPPEs that did not reveal zones of inhibition or revealed no migration of the antifungal components can be seen in the Appendix in Figures 16-18. The 3 NPPEs that showed multiple zones can be seen in Appendix Figure 19.

The 3 NPPEs that showed zones of inhibition either had spots with low  $R_f$  values ( $\leq 0.3$ ) or  $R_f$  values that were numerically close (Appendix Figure 19). Therefore, the TLC separations were repeated with a solvent system of PetEt:EtOAc in a ratio of 7:3. This was done as an attempt to improve spot separation and further distinguish the  $R_f$



values from each other. Increasing separation between compounds would also would directly reduce contamination between individual components when they are isolated with prep-TLC. The bioautography results from the improved TLC separations can be seen in Figure 3.4.2. All  $R_f$  values were increased, and spot separation dramatically improved for two of the NPPEs. Thus, the  $R_f$  values were varied enough to identify each individual TLC band leading to prep-TLC being a feasible procedure to purify the active anticryptococcal components of the NPPEs from the full extract.

Ideally, at least one zone of inhibition would be visualized for each NPPE subjected to this assay. However, due to the conditions used for this particular bioautography assay, an inhibition zone might not be visualized for a few reasons. The original spot on the TLC plate should reveal a zone of inhibition if the active component did not separate under these TLC conditions but is potent enough to diffuse through the agar layer to *C. neoformans*. It is possible that the agar layer over the TLC plate was too thick, thus reducing the diffusion potential of the component and its effect on *C. neoformans*. This lack of inhibition could also be due to synergistic effects between components, meaning lower or no biological activity will be seen with the individual components since two or more are required to inhibit *C. neoformans*.

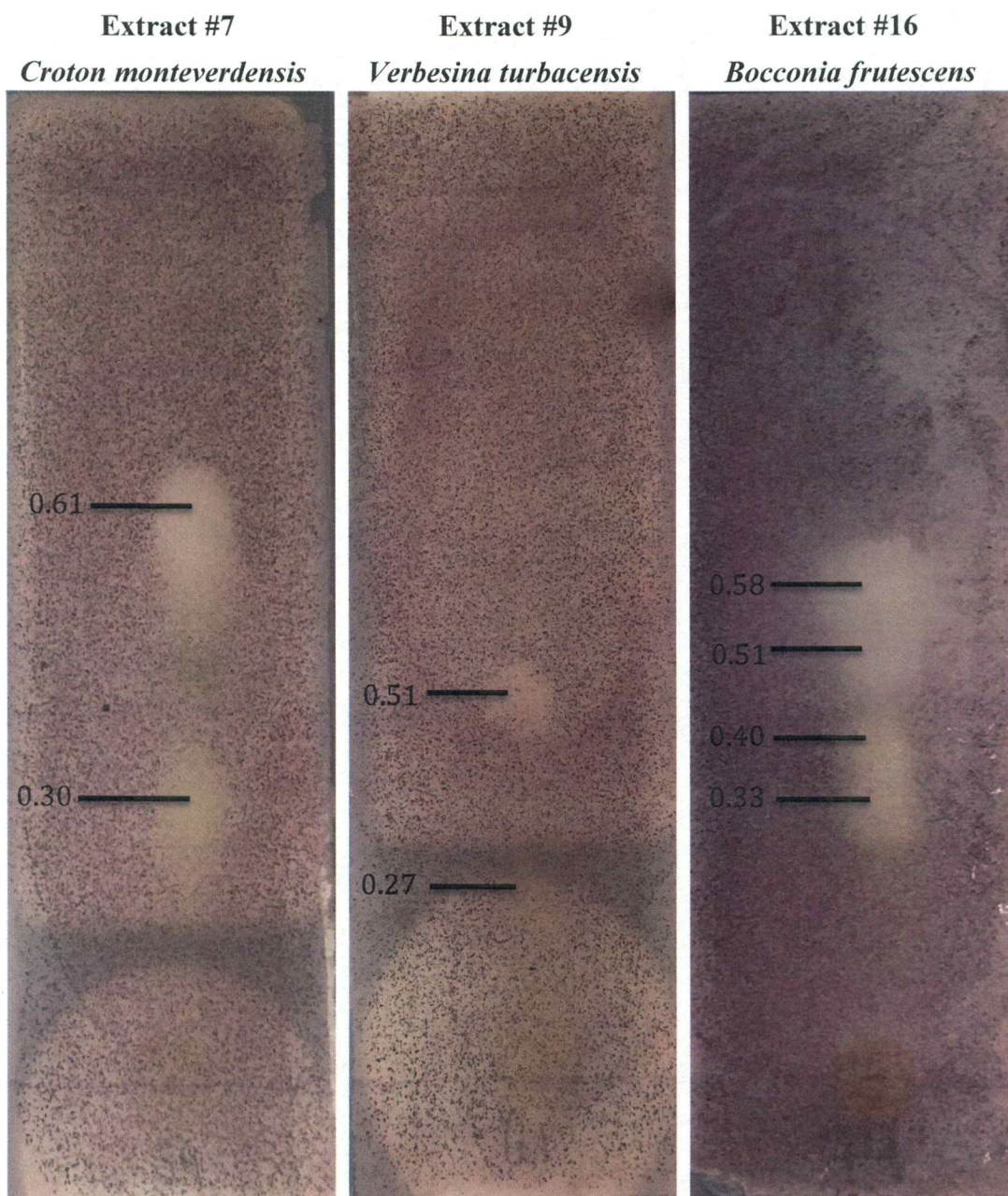


**Figure 3.4.1** Images of agar-overlay bioautography for NPPEs #7, #9, and #16 after staining with INT dye for 48 hours. The appearance of obvious inhibition zones after separation suggests that the components are in high enough concentration to inhibit fungal growth. Calculated  $R_f$  values are shown in black with lines pointing to their corresponding inhibition zone.

### 3.5 Microdilution Assay with Prep-TLC Isolates

Prep-TLC isolates were subjected to the microdilution assay with *C. neoformans* (24067) in order to determine the MIC value. Both zones from extracts #7 and #9 were tested, as well as all 4 of the zones from extract #16. The results from this assay are shown in Figure 3.5 with MIC values listed in Table 3.5.

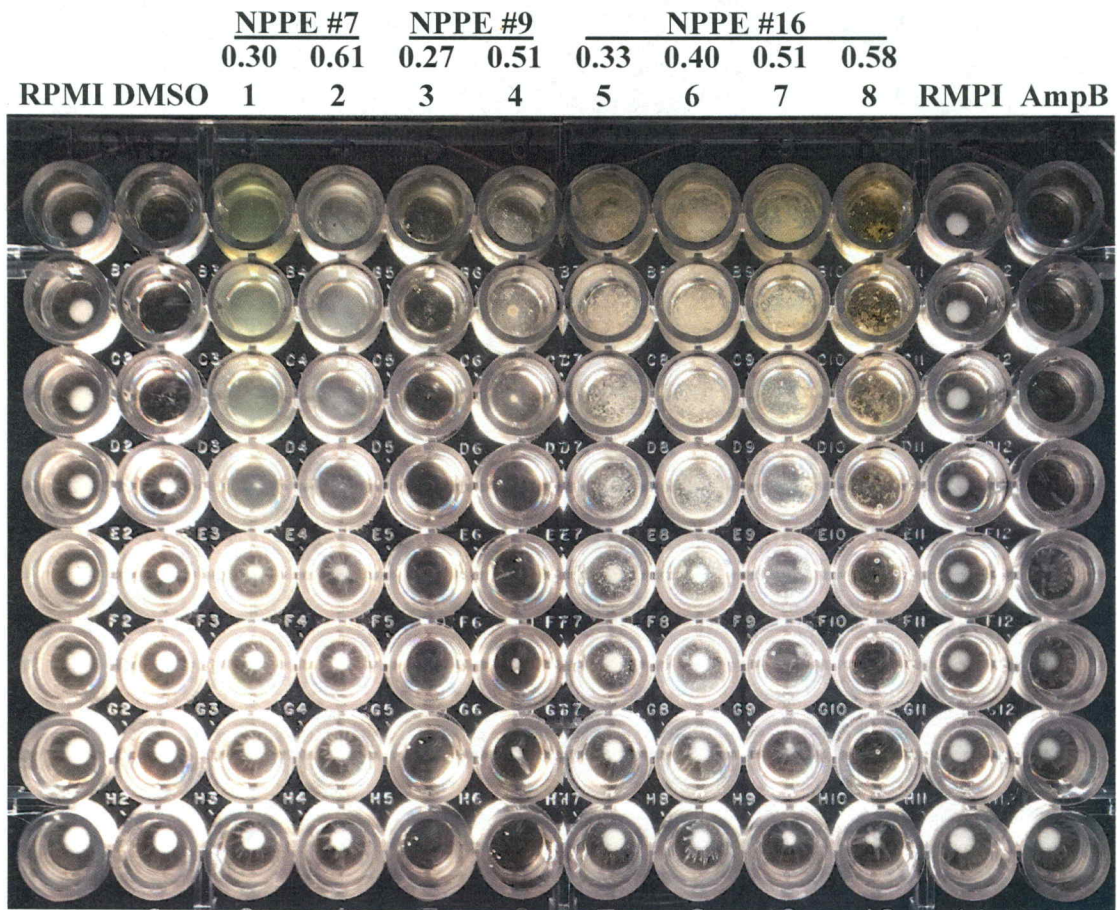


**Figure 3.5** Microdilution assay results from the 8 prep-TLC isolates and the controls with *C. neoformans* (24067) in a 96-well plate. Both RPMI media controls containing only cells grew, showing that cells were healthy. All samples and controls were added to the first row in each column and serially diluted down the column. The small, white clumps in the middle of each well are growth of *C. neoformans*. The fluffy, grainy, or cloudy appearances in some of the wells are due to insoluble solids from the NPPEs.

Because the prep-TLC isolates are assumed single components, the MIC values were calculated in mg/mL as opposed to ppm like the whole bark extracts. The negative control, pure DMSO, inhibited *Cryptococcus neoformans* (24067) at 12.5%, while the positive control, 100  $\mu$ M AmpB, inhibited the fungus at a concentration of 1  $\mu$ M. The RPMI media control exhibited normal cell growth in all wells. If the isolated compound showed activity at a low concentration, identification was pursued. The cutoff for identification was set to 0.16 mg/mL based on literature (Surapuram et al. 2014).

**Table 3.5** Results from the microdilution assay for prep-TLC isolates against *Cryptococcus neoformans* (24067). The observed MIC value in mg/mL is shown in the right column. Results were interpreted visually from the 96-well MIC plates based on growth of the fungus.

Prep-TLC Isolate Number	Extract Plant Name (Number)	R <sub>f</sub> Value	MIC (mg/mL) with <i>C. neoformans</i> (24067)
1	<i>Croton monteverdensis</i> (7)	0.30	0.31
2	<i>Croton monteverdensis</i> (7)	0.61	0.31
3	<i>Verbesina turbacensis</i> (9)	0.27	0.02
4	<i>Verbesina turbacensis</i> (9)	0.51	0.02
5	<i>Bocconia frutescens</i> (16)	0.33	0.62
6	<i>Bocconia frutescens</i> (16)	0.40	0.62
7	<i>Bocconia frutescens</i> (16)	0.51	0.08
8	<i>Bocconia frutescens</i> (16)	0.58	0.04

### 3.6 Structure Determination for Prep-TLC Isolates

Both NMR spectroscopy and GC-MS were utilized to identify the prep-TLC isolates. NMR spectra for each sample consisted of a proton, a HSQC, a HMBC, and a COSY. These spectra were used to determine the structure of the sample by evaluating proton and carbon connections. GC-MS was used to acquire retention times and molecular masses.

#### 3.6.1 NMR Results

Proton, HSQC, HMBC, and COSY spectra were collected to evaluate the structure of select prep-TLC isolates. Only prep-TLC isolates with a MIC value  $\leq 0.16$  mg/mL were subjected to NMR spectroscopy. Coupling constant and multiplicity data were obtained from the proton spectra. Direct proton-carbon connections were determined using the HSQC spectra. The HMBC spectra were used to resolve quaternary carbons. The COSY spectra were used to confirm proton-carbon connections seen in HSQC and HMBC. Proton spectra for all samples are shown below as Figures 3.6.1.A, 3.6.1.B, 3.6.1.C, and 3.6.1.D. The remaining spectra (HSQC, HMBC, and COSY) are shown in Appendix Figures 20-25.

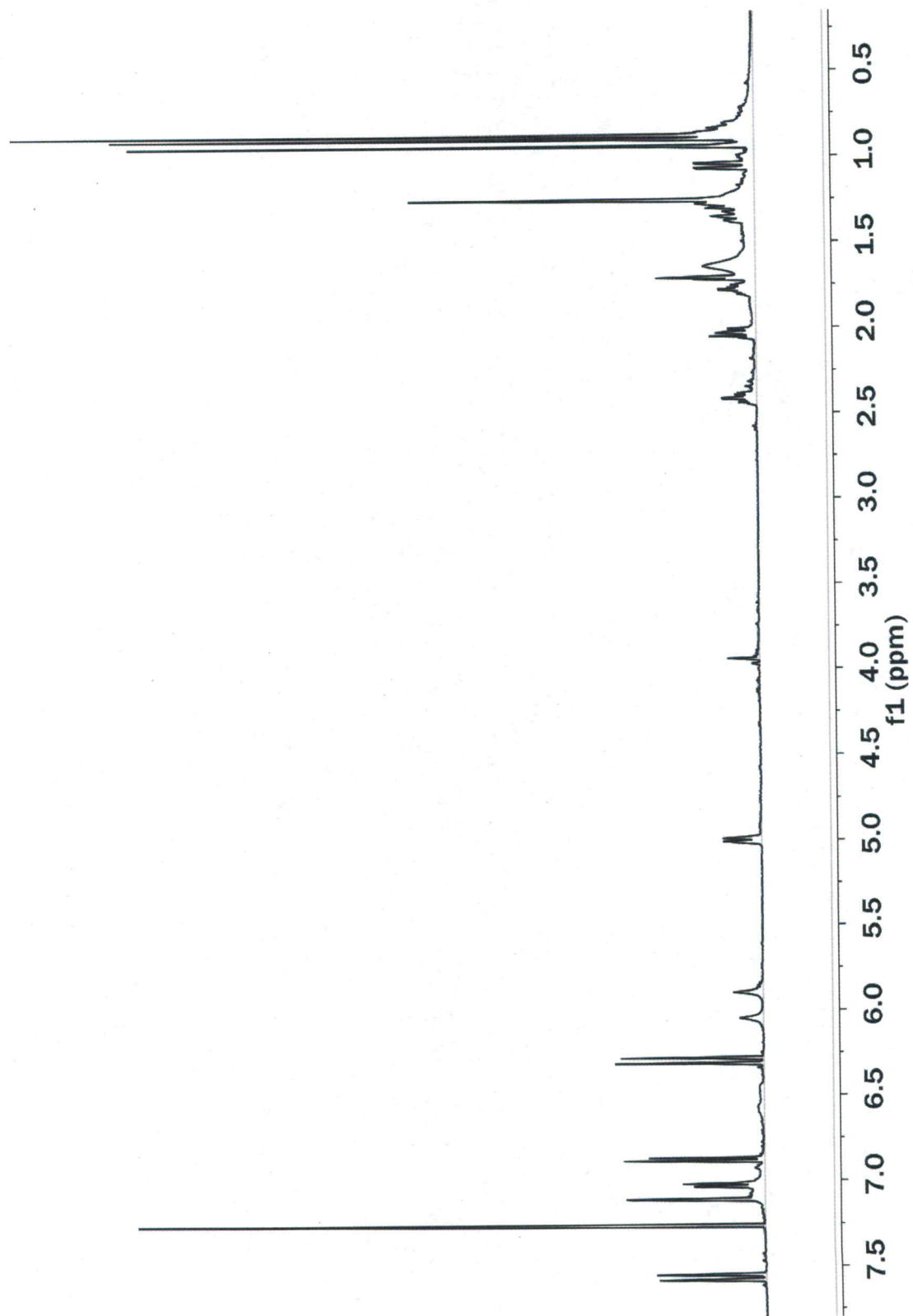


**Figure 3.6.1.A** The 500 MHz <sup>1</sup>H NMR spectrum for  $R_f = 0.27$  from extract #9 in  $\text{CDCl}_3$  (7.26 ppm). Sample concentration was 5 mg/mL.

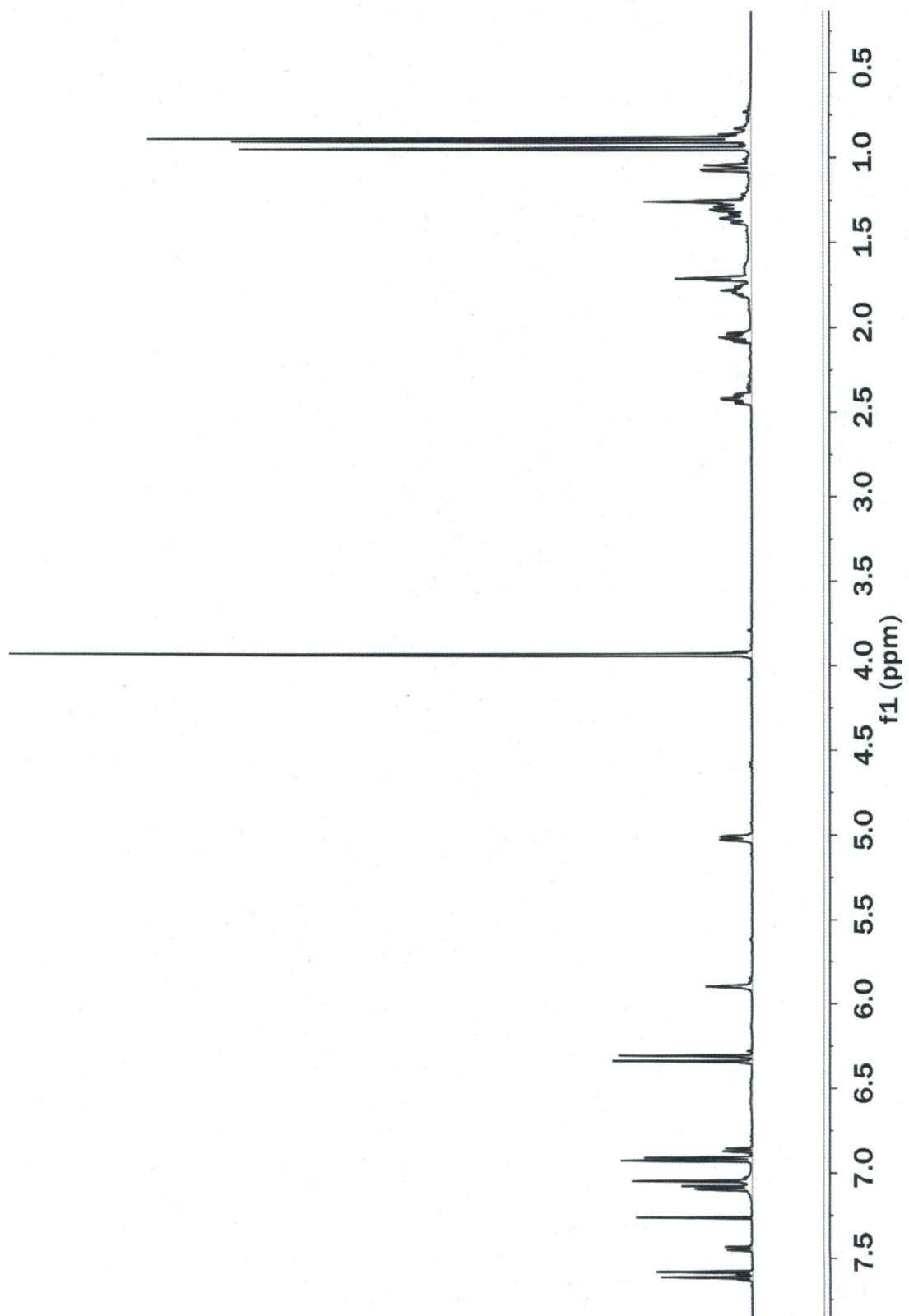


**Figure 3.6.1.B** The 500 MHz  $^1\text{H}$  NMR spectrum for  $R_f = 0.51$  from extract #9 in  $\text{CDCl}_3$  (7.26 ppm). Sample concentration was 5 mg/mL.

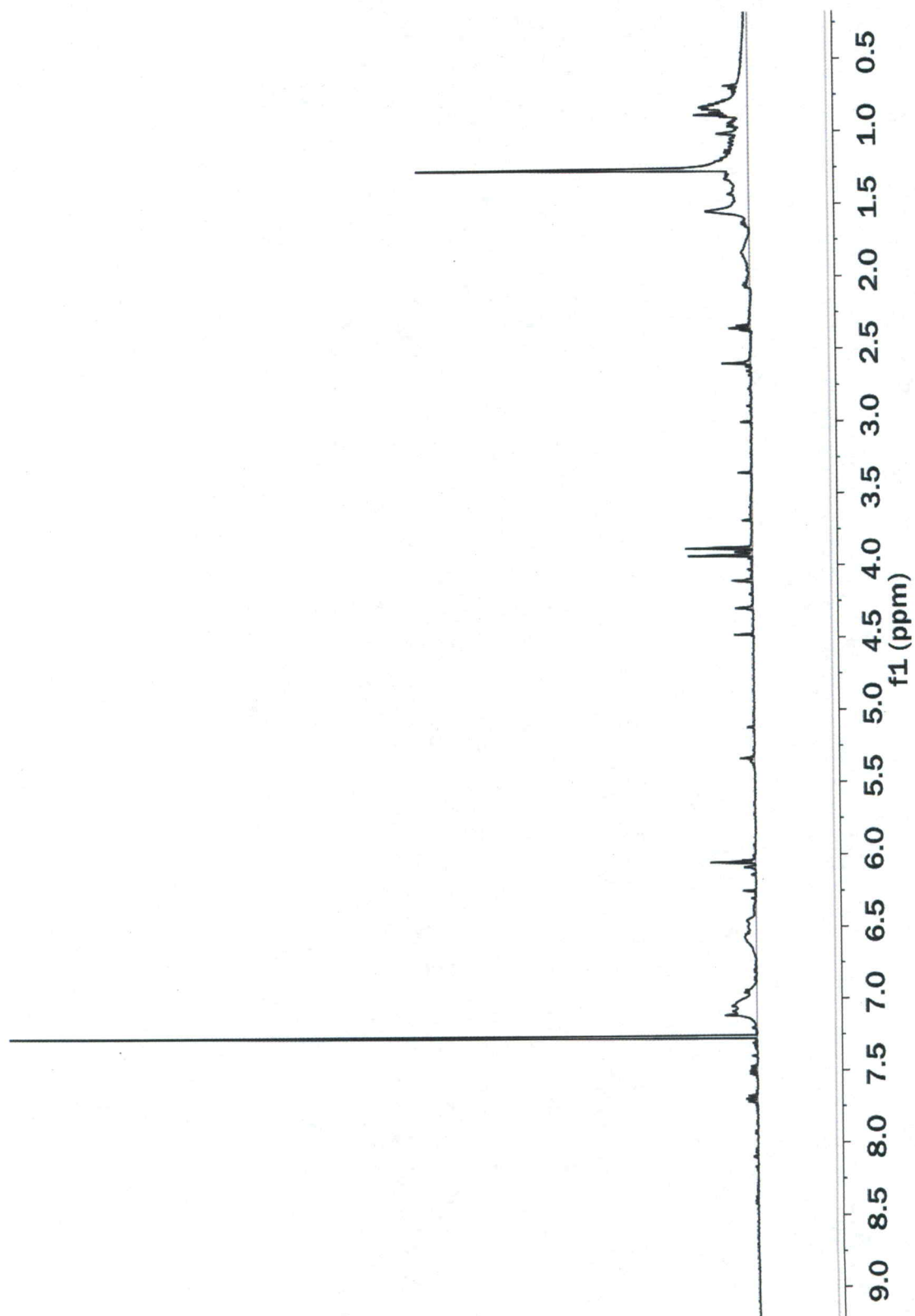


**Figure 3.6.1.C** The 500 MHz <sup>1</sup>H NMR spectrum for R<sub>f</sub> = 0.51 from extract #16 in CDCl<sub>3</sub> (7.26 ppm). Sample concentration was 5 mg/mL.



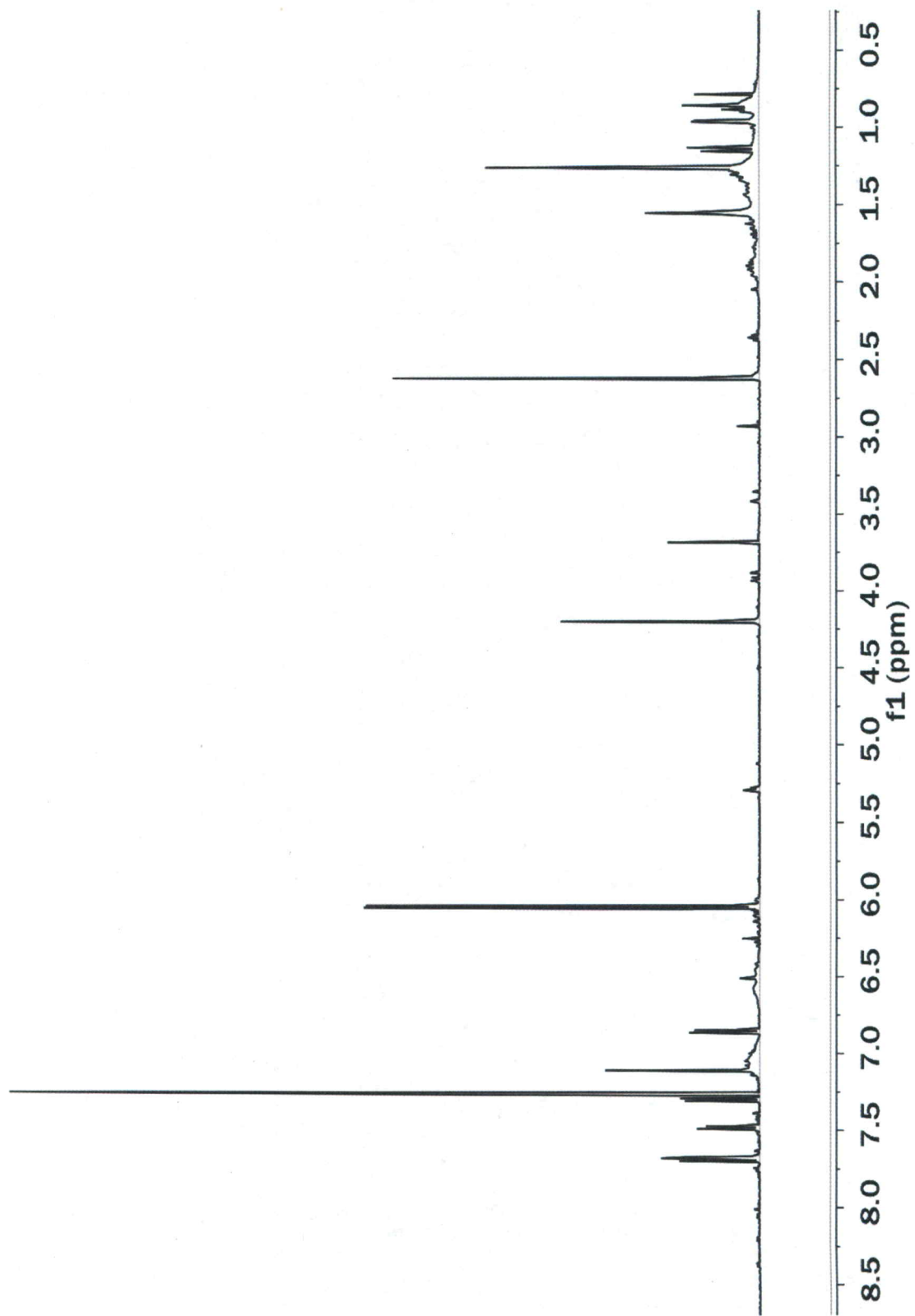


**Figure 3.6.1.D** The 500 MHz <sup>1</sup>H NMR spectrum for R<sub>f</sub> = 0.58 from extract #16 in CDCl<sub>3</sub> (7.26 ppm). Sample concentration was 5 mg/mL.

### **3.6.2 GC-MS Results**

Since the final goal of the study is to identify plant compounds that are potent anticryptococcal agents, GC-MS was implemented to obtain a retention time and a molecular mass for the prep-TLC isolates. The mass-to-charge ratio graphs are shown below in Figures 3.6.2.A, 3.6.2.B, 3.6.2.C, 3.6.2.D. The combined data, including the observed retention times and molecular masses, for the 4 prep-TLC isolates are listed below in Table 3.6.2.

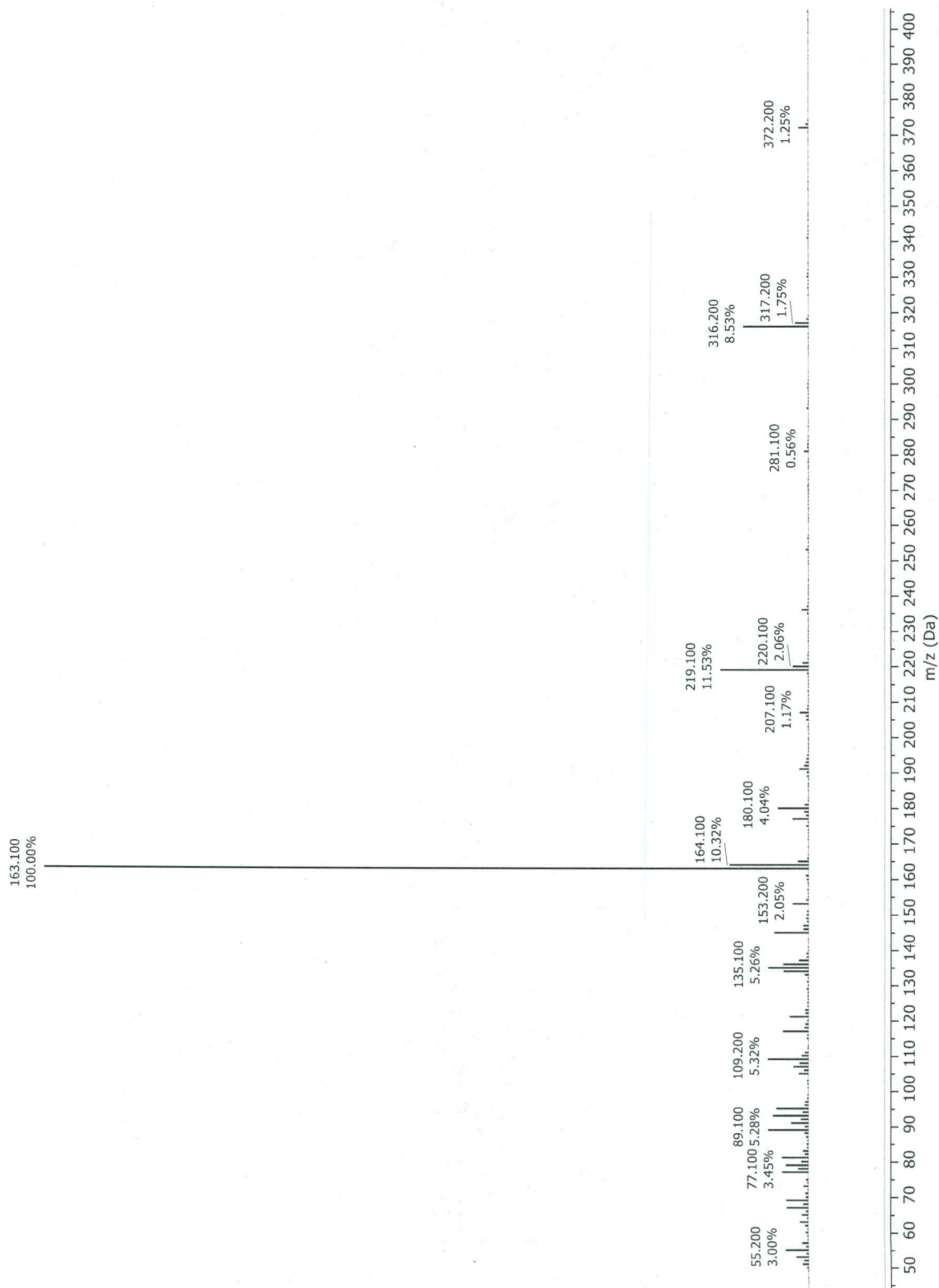


**Figure 3.6.2.A** Mass-to-charge ratio graph of  $R_f = 0.27$  from extract #9. The retention time of this peak was 43 minutes. Peaks are labeled with corresponding mass-to-charge ratio in Daltons as well as their percent intensity.

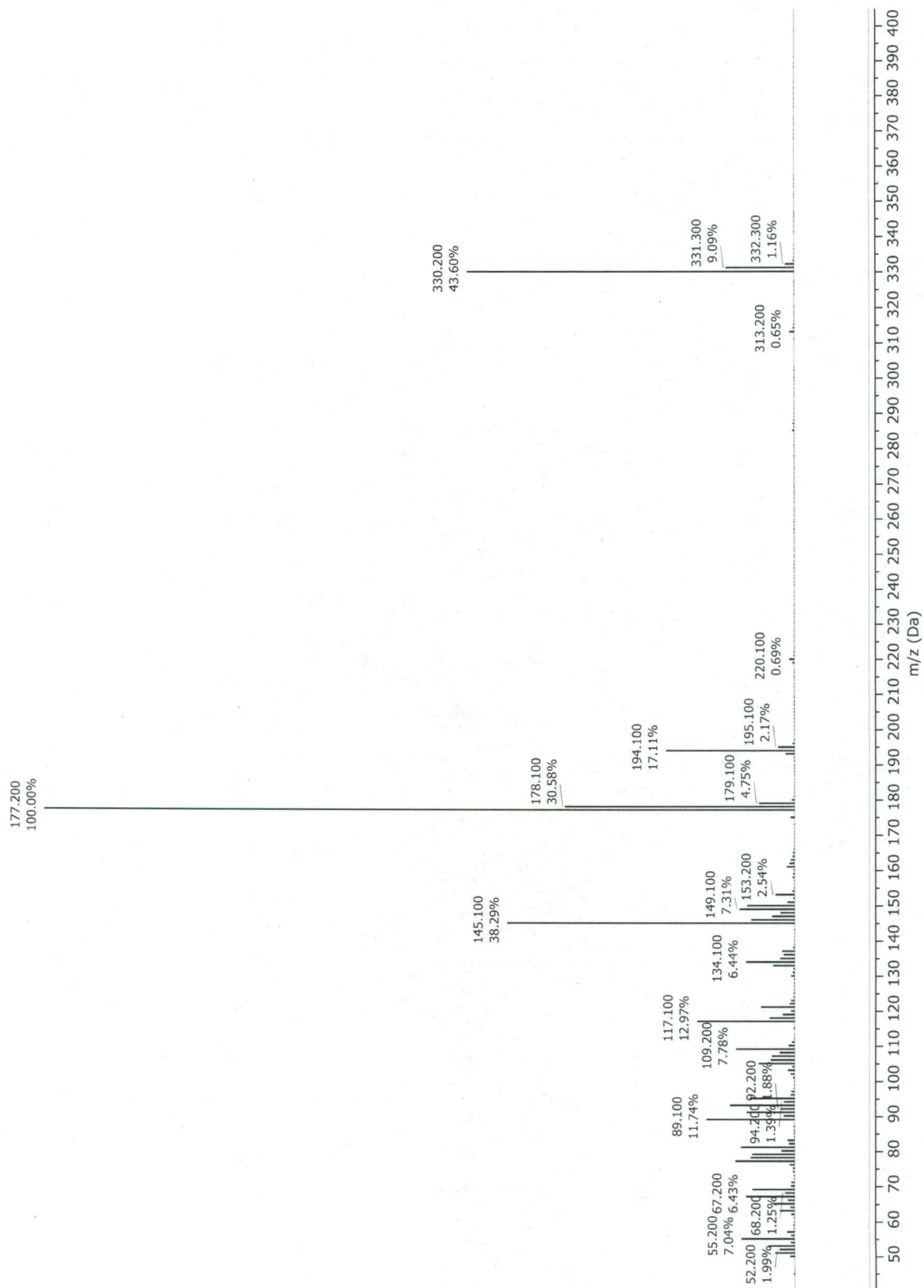


**Figure 3.6.2.B** Mass-to-charge ratio graph of  $R_f = 0.51$  from extract #9. The retention time of this peak was 44 minutes. Peaks are labeled with corresponding mass-to-charge ratio in Daltons as well as their percent intensity.

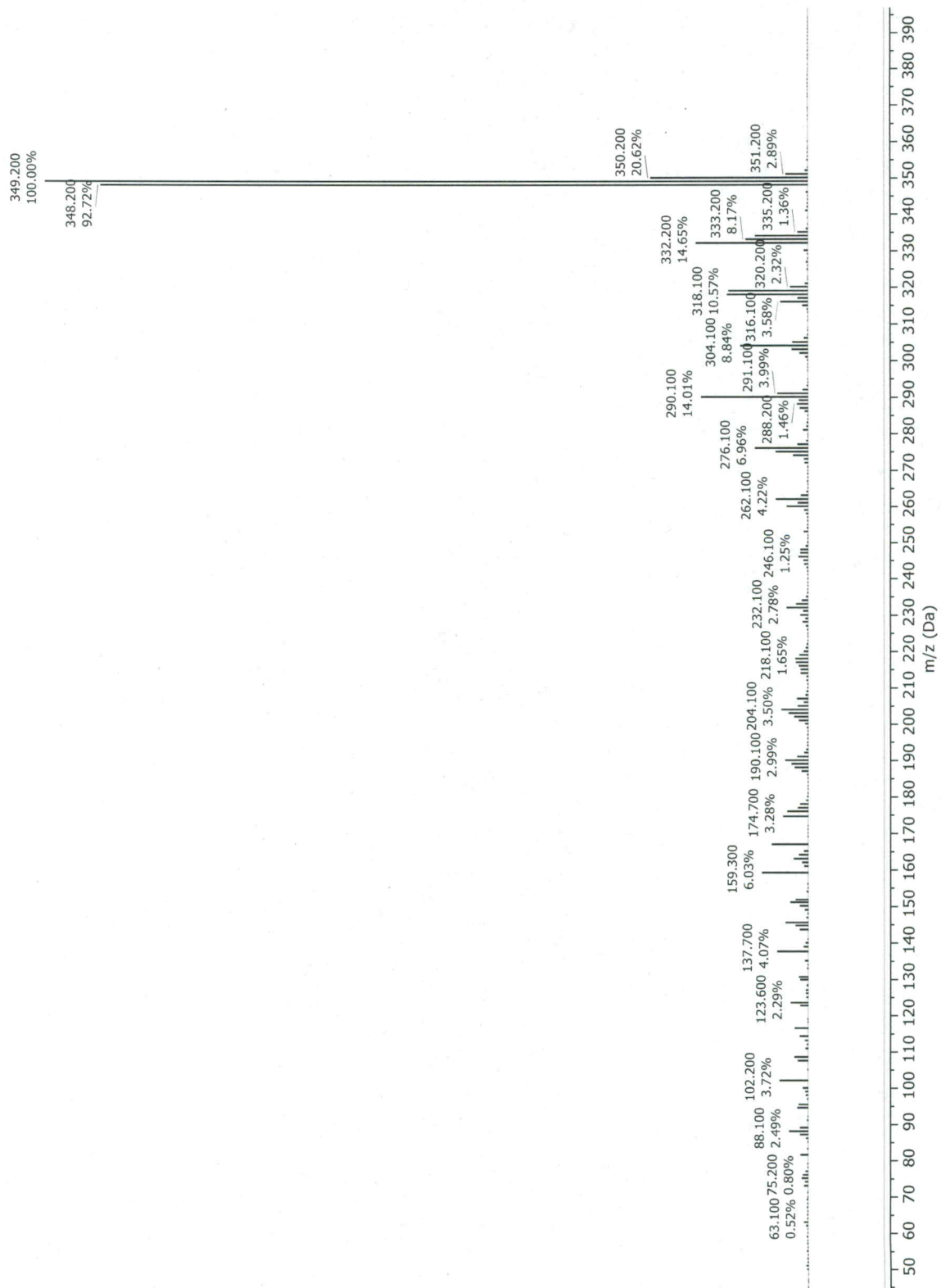


**Figure 3.6.2.C** Mass-to-charge ratio graph of  $R_f = 0.51$  from extract #16. The retention time of this peak was 41 minutes. Peaks are labeled with corresponding mass-to-charge ratio in Daltons as well as their percent intensity.

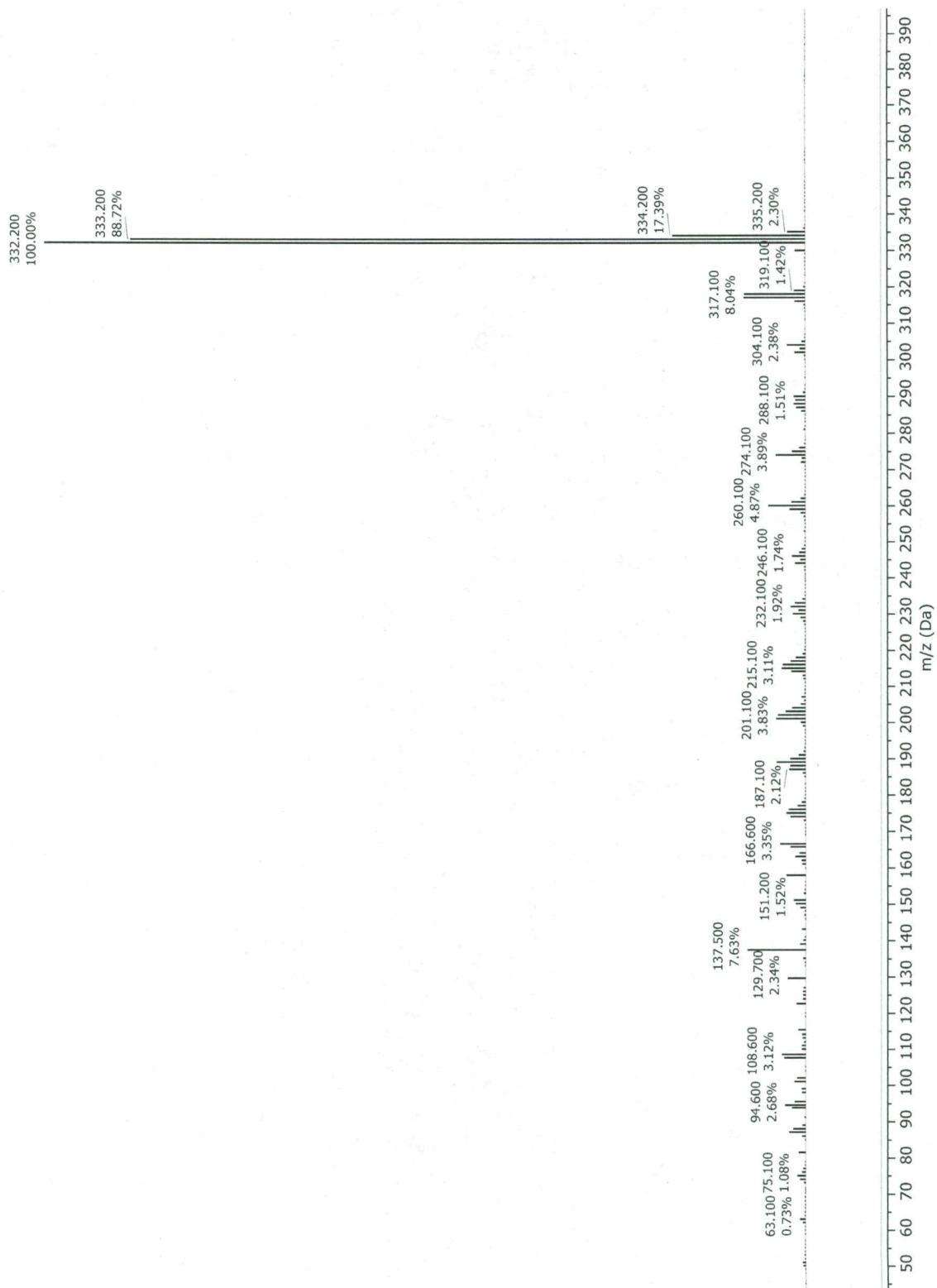


**Figure 3.6.2.D** Mass-to-charge ratio graph of  $R_f = 0.58$  from extract #16. The retention time of this peak was 42 minutes. Peaks are labeled with corresponding mass-to-charge ratio in Daltons as well as their percent intensity.

**Table 3.6.2** Summary of the GC-MS results for the 4 prep-TLC isolates. Molecular mass reflects that of the mass at the corresponding retention time.

Prep-TLC Isolate Number	Extract Plant Name (Number)	R <sub>f</sub> Value	Retention Time (minutes)	Molecular Mass (g/mol)
3	<i>Verbesina turbacensis</i> (9)	0.27	40.74	316.2
4	<i>Verbesina turbacensis</i> (9)	0.51	38.97	330.2
7	<i>Bocconia frutescens</i> (16)	0.51	44.14	349.2
8	<i>Bocconia frutescens</i> (16)	0.58	43.89	332.2

### 3.6.3 Prep-TLC Isolate Identification

Prep-TLC isolate #3 was identified as the bornyl hydroxycinnamic ester, bornyl caffeate (Figure 3.6.3.A). This identification was made based on NMR peak assignments (Table 3.6.3.A) and the molecular mass obtained from GC-MS analysis. Prep-TLC isolate #4 was identified as bornyl caffeate methoxy derivative, bornyl ferulate (Figure 3.6.3.B). This identification was also made based on NMR peak assignments (Table 3.6.3.B) and the molecular mass. Prep-TLC isolates #7 and #8 have yet to be identified due to sample impurities leftover from prep-TLC, as observed in the proton NMR spectra shown above in Figures 3.6.1.C and 3.6.1.D, respectively.





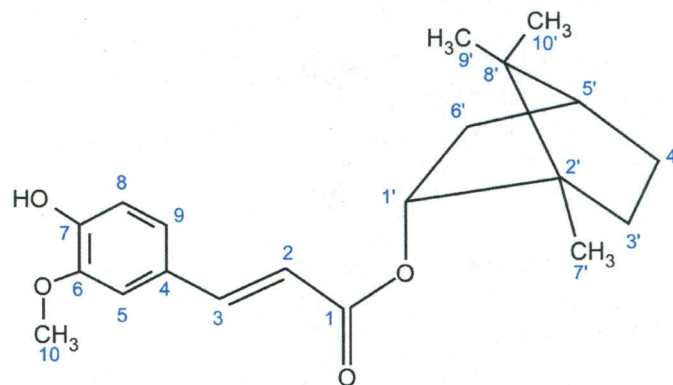


**Figure 3.6.3.B** Chemical structure of bornyl ferulate. Blue numbers correspond to the respective carbon atom.

**Table 3.6.3.B** NMR assignments for  $R_f = 0.51$  from extract #9. Positions correspond to structure of identified compound (as shown in Figure 3.6.3.B).  $\delta C$ , multiplicity information was extrapolated from HSQC and HMBC spectra.

Position	$\delta C$ , multiplicity	$\delta H$ (J, Hz)	HMBC (H $\rightarrow$ C)	COSY
1	167.69, C	--	3	--
2	116.12, CH	6.32, d (15.89)	--	3
3	144.33, CH	7.59, d (15.89)	5; 9	2
4	127.09, C	--	2; 8	--
5	109.30, CH	7.04, d (1.83)	3; 9	10
6	147.85, C	--	5; 9	--
7	146.75, C	--	5; 8	--
8	114.71, CH	6.92, d (8.10)	9	9
9	123.02, CH	7.08, dd (1.83, 8.17)	3; 5; 8	8
10	55.96, CH <sub>3</sub>	3.93, s	--	5
1'	79.85, CH	5.01, m	7'	3'; 6'
2'	47.84, C	--	7'; 9'; 10'	--
3'	27.26, CH <sub>2</sub>	1.35, m; 2.05, m	5'; 7'	1'; 4'; 3'; 5';
4'	28.07, CH <sub>2</sub>	1.28, m; 1.78, m	--	6'
5'	44.94, CH	1.71, t (4.43, 4.43) 1.05, dd (3.51, 13.75);	9'; 10'	4'; 6'; 1'; 4';
6'	36.86, CH <sub>2</sub>	2.42, m	--	5'
7'	13.56, CH <sub>3</sub>	0.88, s	--	--
8'	48.94, C	--	5'; 7'; 9'; 10'	--
9'	18.88, CH <sub>3</sub>	0.94, s	10'	10'
10'	19.73, CH <sub>3</sub>	0.90, s	9'	9'

## CHAPTER 4

### CONCLUSIONS AND FUTURE WORK

#### 4.1 Conclusions

A growing consequence of modern medicine is the negative impacts that drug resistance has bestowed on the medical community. Due to various reasons, growing spikes in drug resistance can be seen throughout the spectrum of pathogenic microorganisms, fungi included. Specifically in *Cryptococcus* species, there has been a notable rise in antifungal resistance as well as infection rates worldwide over the past decade (Rajasingham et al. 2017). As an example, the rise of cryptococcal meningitis infection in HIV/AIDS patients in sub-Saharan Africa has climbed so dramatically that it has surpassed tuberculosis in mortality rates (Brown et al. 2012). Considering both the increasing rates of infection and antifungal resistance of *Cryptococcus*, it is absolutely dire that new anticryptococcal agents are discovered.

Since plants offer seemingly endless sources of medically promising biologically active compounds and are renewable resources, they serve as excellent candidates for the grounds of new drug discovery. To accomplish analyzing plant matter for relative and novel active compounds, bioautography and preparative-TLC are complimentary procedures that allow for the biologically active component(s) from a mixture to be determined. Subsequent identification of active compounds is facilitated by the combine

isolation coupled to activity determination. Thus, in weeks to months, this entire process can be completed and lead to newly characterized biologically active compounds.

This process was applied to 16 NPPEs from Monteverde, Costa Rica. The NPPEs were initially analyzed for anticryptococcal activity. From this analysis, 14 out of the 16 were found to strongly inhibit growth of the fungus. Due to limited availability, only 12 of the 16 extracts were further analyzed for their biologically active component(s). From bioautography, 3 of the 12 extracts showed a separable zone of inhibition, 3 showed a zone of inhibition over the original spot on the TLC plate, and 6 did not show a zone of inhibition. Subsequent prep-TLC was performed to separate and isolate the active components from the 3 extracts that showed separable zones of inhibition. A total of 8 different compounds were collected using prep-TLC from the 8 zones of inhibition visualized from the 3 extracts. The anticryptococcal activity of the 8 prep-TLC isolates was evaluated, revealing that 4 out of the 8 strongly ( $\leq 0.16$  mg/mL) inhibited the growth of *C. neoformans* (24067). Using NMR spectroscopy and GC-MS, 2 of the 4 prep-TLC isolates were identified, however 2 still remain to be identified. The 2 prep-TLC isolates from the plant *Verbesina turbacensis* were identified as bornyl caffeate and bornyl ferulate. The 2 prep-TLC isolates from *Bocconia frutescens* require further purification before identification, a process that is currently underway.

Previous literature reports both of the bornyl compounds to be inhibitors of the trypanosome cysteine protease (Ogungbe et al. 2010). To our knowledge, this is the first report illuminating the potent anticryptococcal activity, and thus the first insights to antifungal activity, of the two bornyl hydroxycinnamic esters bornyl caffeate and bornyl ferulate. Also, this is the first report elaborating the anticryptococcal activity of the acetone bark extracts of plants *Verbesina turbacensis* and *Bocconia frutescens*.

It is interesting to note that out of the 16 NPPEs evaluated for anticryptococcal activity, 12 completely inhibited growth of *C. neoformans* (24067) at or below an MIC value of 80 ppm. It should also be mentioned that all 16 of the NPPEs showed complete inhibition at a concentration of 315 ppm or lower. This strong activity correlation from a single NPPE data set may be a coincidence since only 16 bark extracts from one region of the globe were screened for activity. However, there may be an underlying cause for why this pathogenic fungus is dramatically susceptible to NPPEs. While this is currently pure speculation, *C. neoformans* may be affected intensely by NPPEs because of how common *C. neoformans* is to outdoor environments across the globe. As the fungus is prevalent in bird excretion and soil, if it was capable of killing most plants, these plants would most likely not exist, or exist under a constant state of infection. Since it can be observed that most plants are not killed by *C. neoformans* infection, or display no obvious signs of infection, the plants must have mechanisms to defend themselves against the fungus. Keeping this in mind, it can be said in good confidence that NPPEs are a promising source of novel anticryptococcal lead compounds and are deserving of attention by the scientific community.

#### **4.2 Future Work**

The main goal for the near future is to identify the remaining two prep-TLC isolates #7 and #8. Most likely this goal will be accomplished through more intense purification steps, either by using a different prep-TLC method or by high performance liquid chromatography (HPLC), in order to completely separate the active compound(s). Once purified, they can be identified using the same methods implemented herein.

Another important goal for the near future is to subject the identified prep-TLC isolates to cytotoxicity assays to determine whether or not the compounds are toxic to humans at relative medical doses. It would be interesting to look at any possible correlations between structure and activity of the compounds if they are close derivatives, like the bornyl compounds. Changing one substituent on a molecule at a time could have an impact on its ability to inhibit *C. neoformans* (24067). This could also have an impact on the cytotoxicity of the molecule. The compounds should eventually be subjected to mechanism-of-action assays in order to evaluate how they are inhibiting the growth. Also, since *C. neoformans* (24067) was the only strain and serotype used in this study, the compounds should be screened against other species of *Cryptococcus* as well as other strains/serotypes of *C. neoformans*. This would be a great starting point to evaluate the potential of the compounds to become a solution for all cryptococcal infections.

In the far future, the prep-TLC isolates should be subjected to various synergy assays with medically relevant compounds such as current antifungals, over-the-counter drugs, and common small molecules. This could identify negative side interactions. This is important because ideally these compounds would progress down the antifungal pipeline and eventually become new therapeutic options for cryptococcal infections. They would most likely be eliminated as drug candidates if they were to cause harmful side reactions with common compounds such as NSAIDs or caffeine.

Other future works could include optimizing TLC and bioautography conditions for the 3 NPPEs that showed a zone of inhibition over the original spot on the TLC plate (#2, #4, and #13). All 3 of the NPPEs had a MIC value of 20 ppm with *C. neoformans* (24067) and should contain at least one component responsible for the activity.

## APPENDIX

UAH NPDDG Number	UAH NPDDG Code	Scientific Name	Thesis Number
51	MABIBA	<i>Machaerium biovalatum</i>	1
52	OCLLBA	<i>Ocotea</i> sp. "los llanos"	2
54	DIDIBE	<i>Diospyros digyna</i>	3
56	PSPABA	<i>Psychotria parvifolia</i>	4
57	CETOBA	<i>Cedrela tonduzii</i>	5
58	LOOLBA	<i>Lonchocarpus oliganthus</i>	6
59	CRMOBD	<i>Croton monteverdensis</i>	7
60	TAMEBE	<i>Tapirira Mexicana</i>	8
61	VETUBA	<i>Verbesina turbacensis</i>	9
63	STMOBC	<i>Styphnolobium monteviridis</i>	10
64	MYBLBD	<i>Myrcianthes</i> sp. "black fruit"	11
67	CUGLBD	<i>Cupania glabra</i>	12
69	ARREBA	<i>Ardisia revoluta</i>	13
70	ERLABD	<i>Erythrina lanceolata</i>	14
73	BUOVBC	<i>Bursera ovalifolia</i>	15
74	BOFRBA	<i>Bocconia frutescens</i>	16

**Table 1** Combined information regarding the NPPEs used for this Thesis. The UAH NPDDG has a specific numbering and coding system for each plant extract they collect, and this is shown in the first two columns respectively. The proper scientific name for each plant species used for extraction is shown in the third column. In the last column, the numbering system is listed that was used for simplicity in this Thesis.

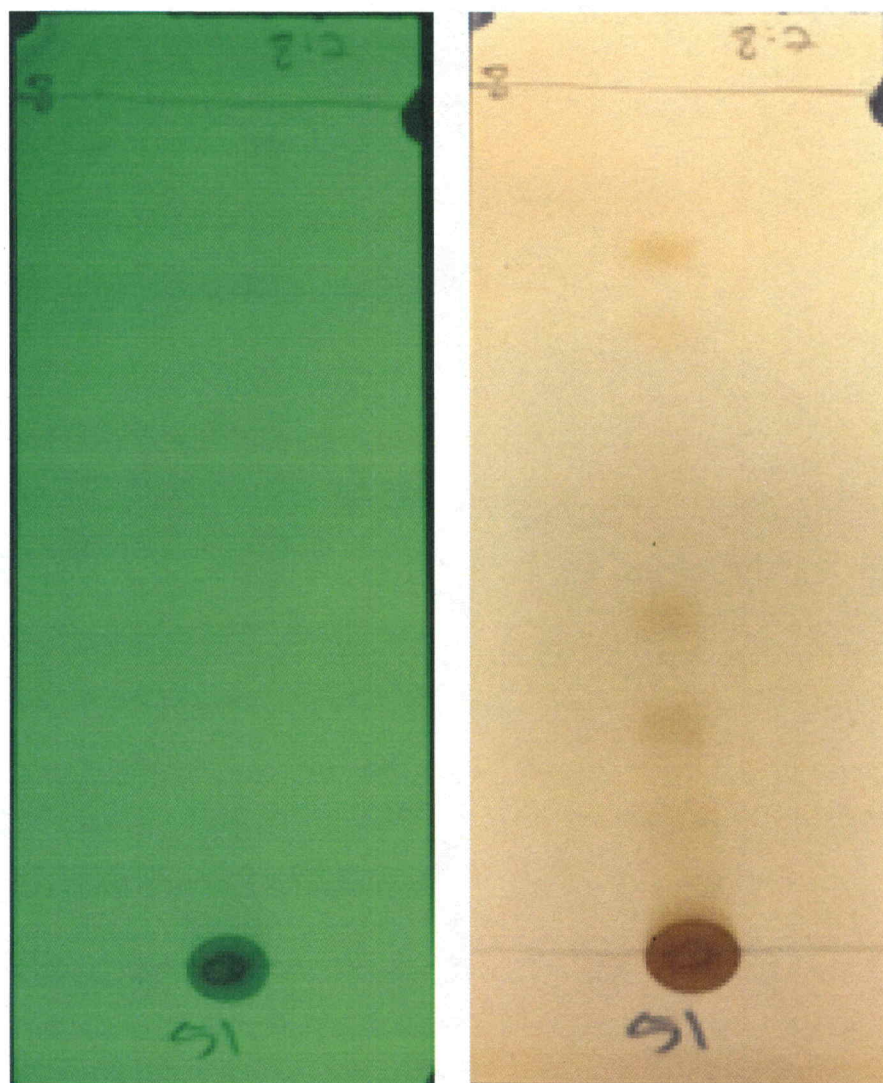


**Figure 1** Visualization of NPPE #1 after separation with 8:2 petroleum ether: ethyl acetate on a silica gel TLC plate. UV light detection is shown on the left, and the 10-minute iodine stain is shown on the right. While UV shows no discernable separation, five faint but different spots can be seen after staining with iodine.

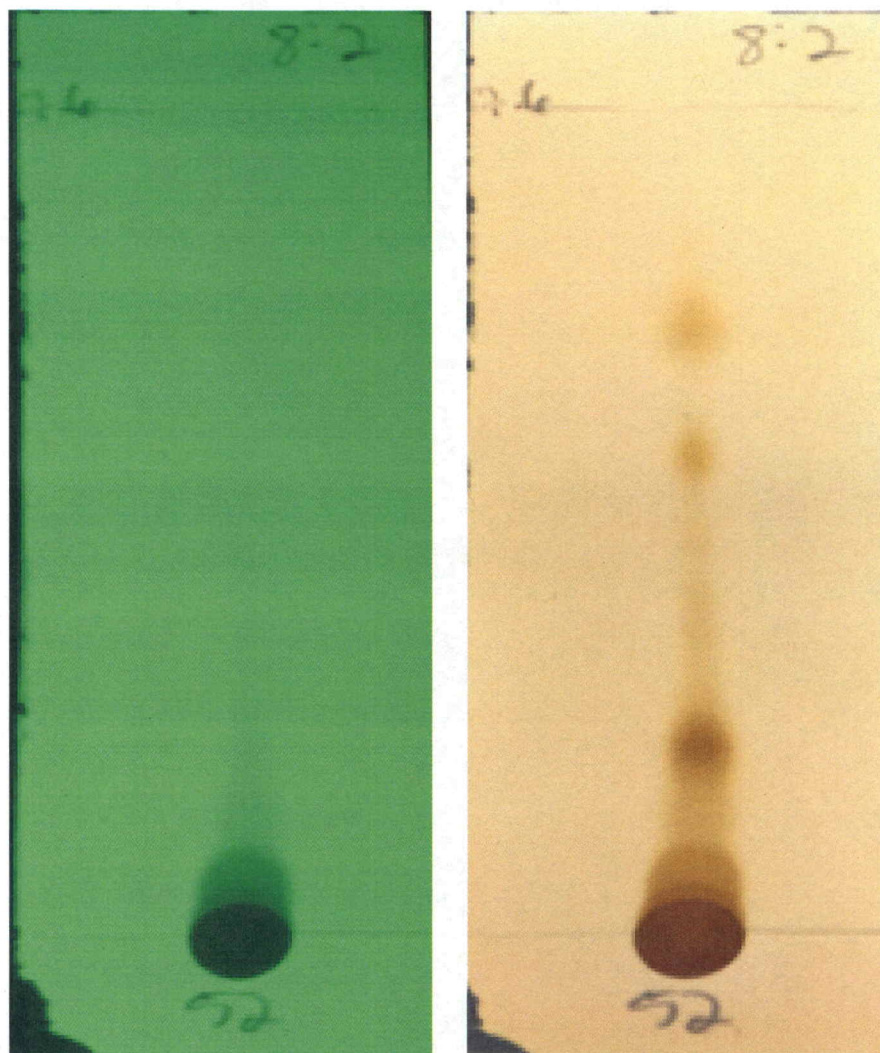


**Figure 2** Visualization of NPPE #2 after separation with 8:2 petroleum ether: ethyl acetate on a silica gel TLC plate. UV light detection is shown on the left, and the 10-minute iodine stain is shown on the right. While UV barely showed discernable separation, three different clear spots were seen after staining with iodine, with a few spots that appear to be bunched together and not completely separated.



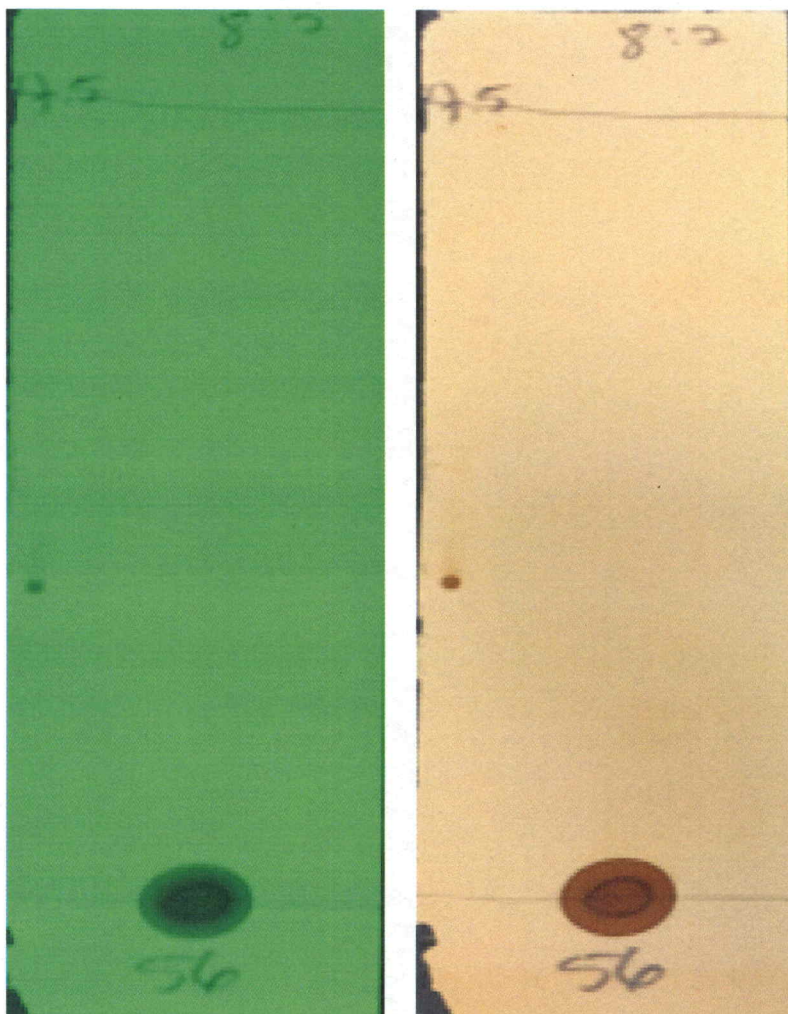


**Figure 3** Visualization of NPPE #4 after separation with 8:2 petroleum ether: ethyl acetate on a silica gel TLC plate. UV light detection is shown on the left, and the 10-minute iodine stain is shown on the right. Neither UV nor the iodine stain showed discernable separation. The tiny spot on the far left of each plate is an artifact and did not arise from solvent separation.

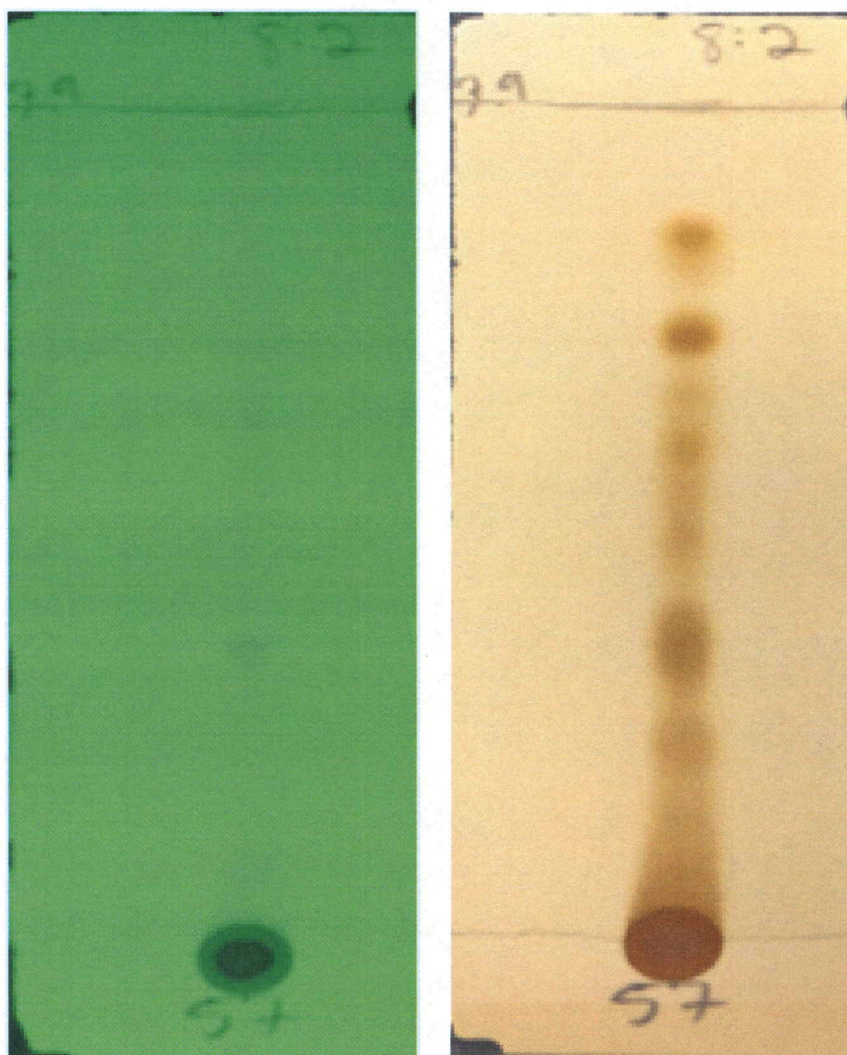


**Figure 4** Visualization of NPPE #5 after separation with 8:2 petroleum ether: ethyl acetate on a silica gel TLC plate. UV light detection is shown on the left, and the 10-minute iodine stain is shown on the right. While UV showed no discernable separation, the iodine stain revealed five distinct spots, with a few spots that appear to be bunched together and not completely separated

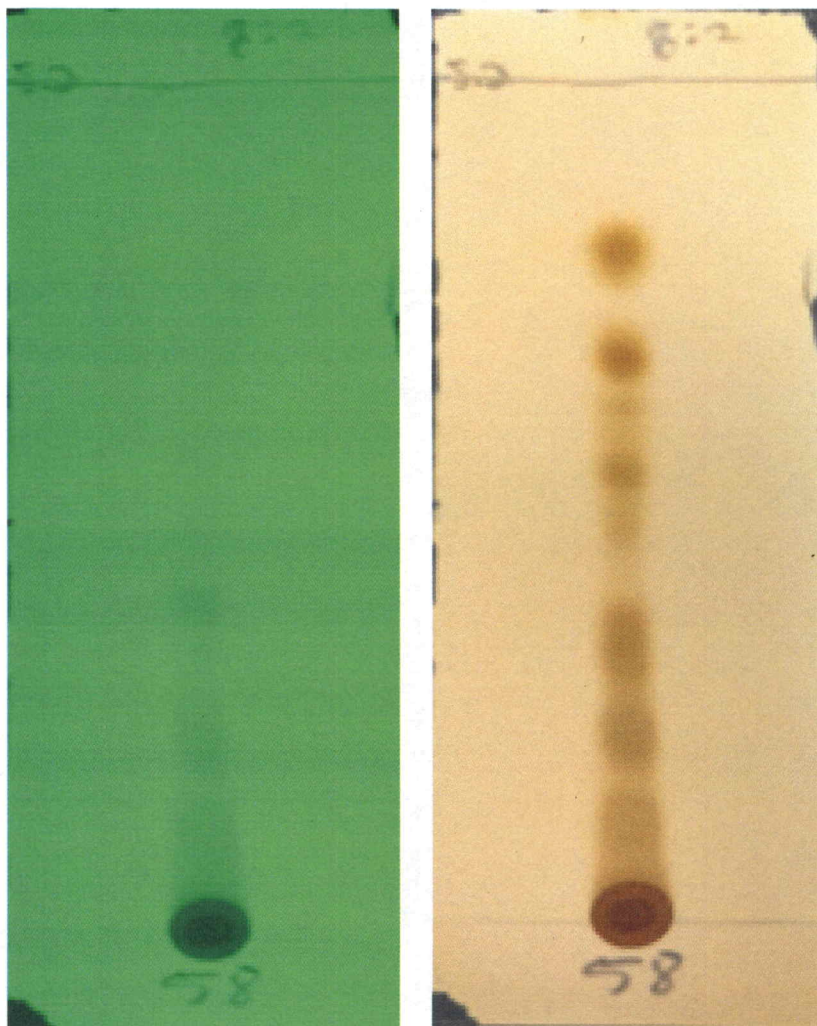


**Figure 5** Visualization of NPPE #6 after separation with 8:2 petroleum ether: ethyl acetate on a silica gel TLC plate. UV light detection is shown on the left, and the 10-minute iodine stain is shown on the right. UV showed two distinct spots, with another spot that appeared to smear and was not completely separated. The iodine stain revealed six distinct spots, with minimal smearing, although the remaining spots seem overlapped with others.

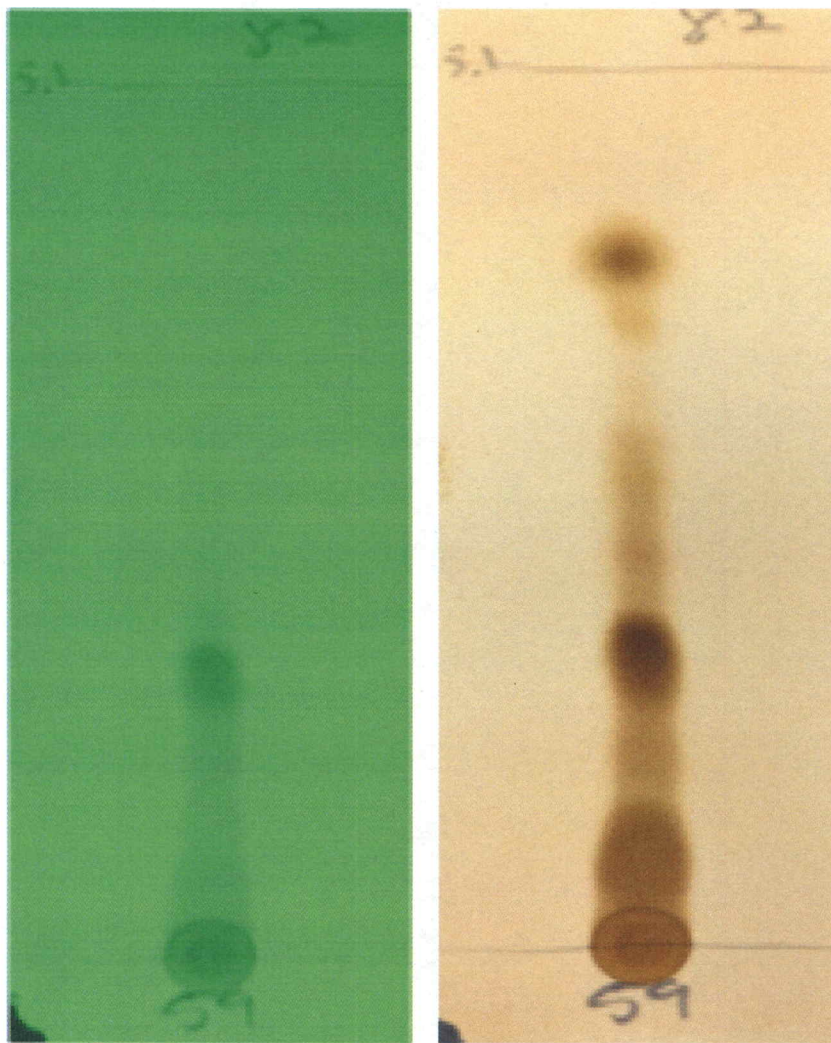


**Figure 6** Visualization of NPPE #7 after separation with 8:2 petroleum ether: ethyl acetate on a silica gel TLC plate. UV light detection is shown on the left, and the 10-minute iodine stain is shown on the right. UV showed one distinct spot, with a few spots that appeared to smear and were not completely separated. The iodine stain revealed three distinct spots, with slight smearing, although the remaining spots seem overlapped with others.

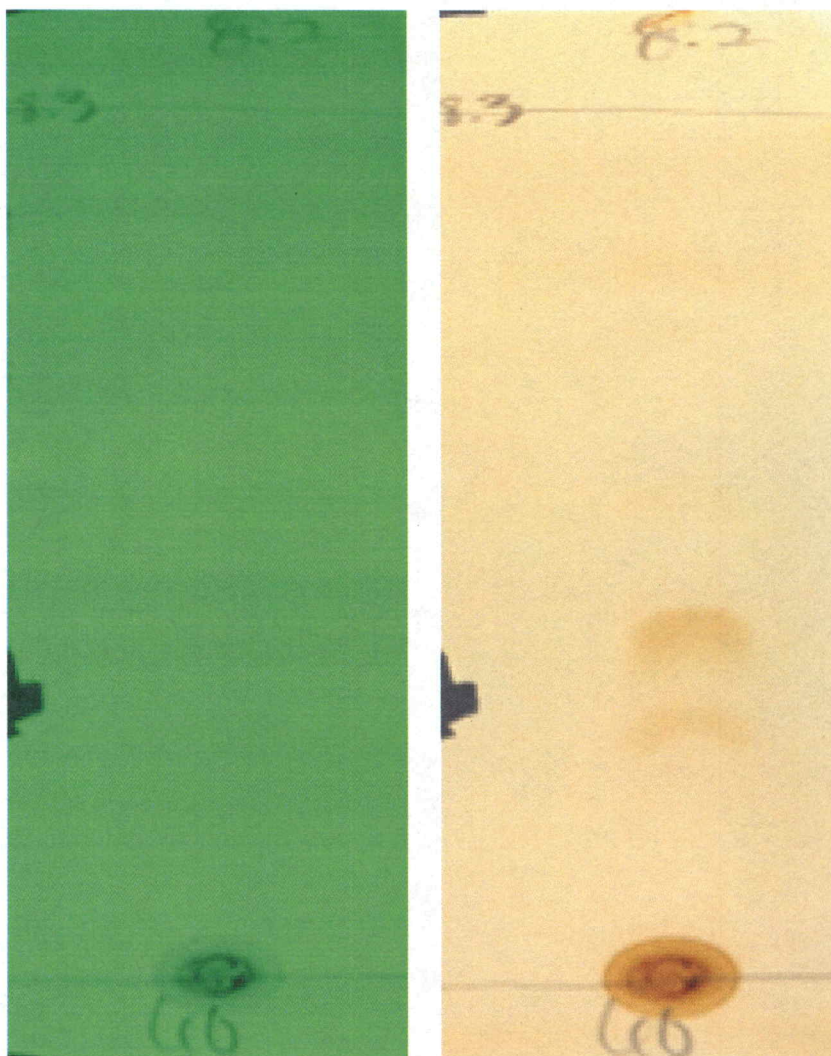


**Figure 7** Visualization of NPPE #8 after separation with 8:2 petroleum ether: ethyl acetate on a silica gel TLC plate. UV light detection is shown on the left, and the 10-minute iodine stain is shown on the right. While UV showed no discernable separation, the iodine stain revealed two distinct spots. Note that product still remains on the starting line, thus indicating complete separation with this solvent system was not achieved.

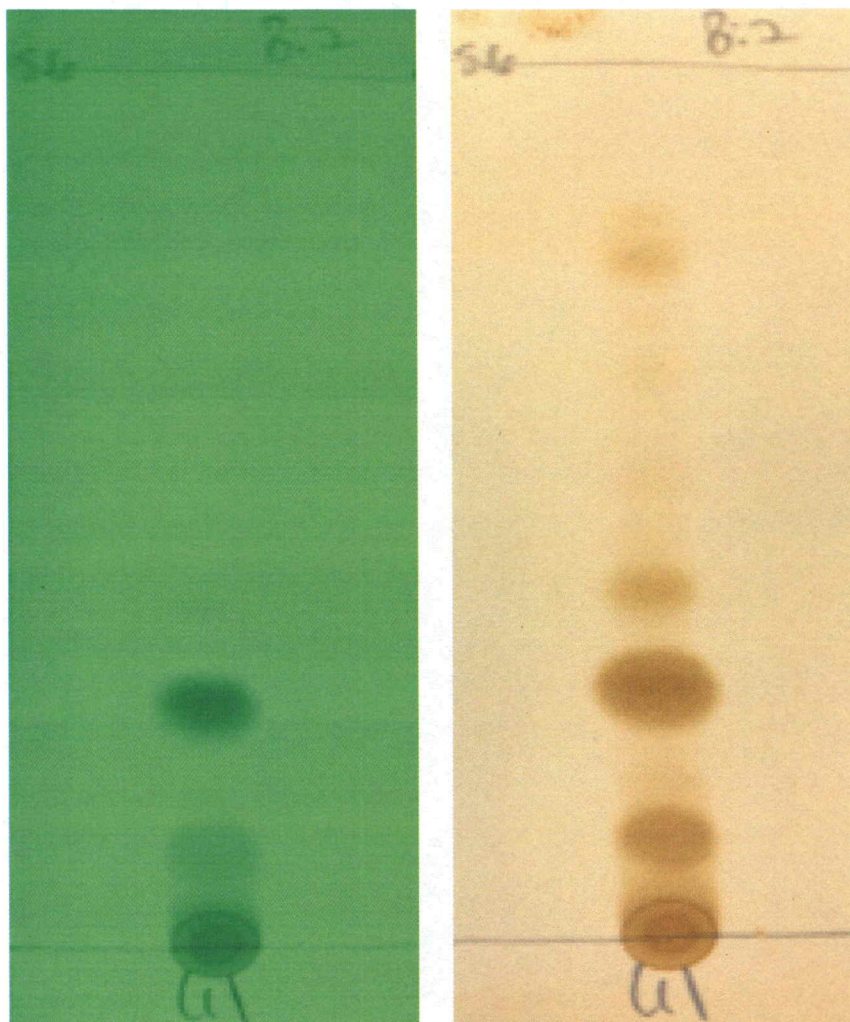


**Figure 8** Visualization of NPPE #9 after separation with 8:2 petroleum ether: ethyl acetate on a silica gel TLC plate. UV light detection is shown on the left, and the 10-minute iodine stain is shown on the right. UV showed two distinct spots, while the iodine stain revealed four distinct spots, with minimal smearing. It appears that there could be other spots judging from the iodine stain, however they are faint and hardly discernible.

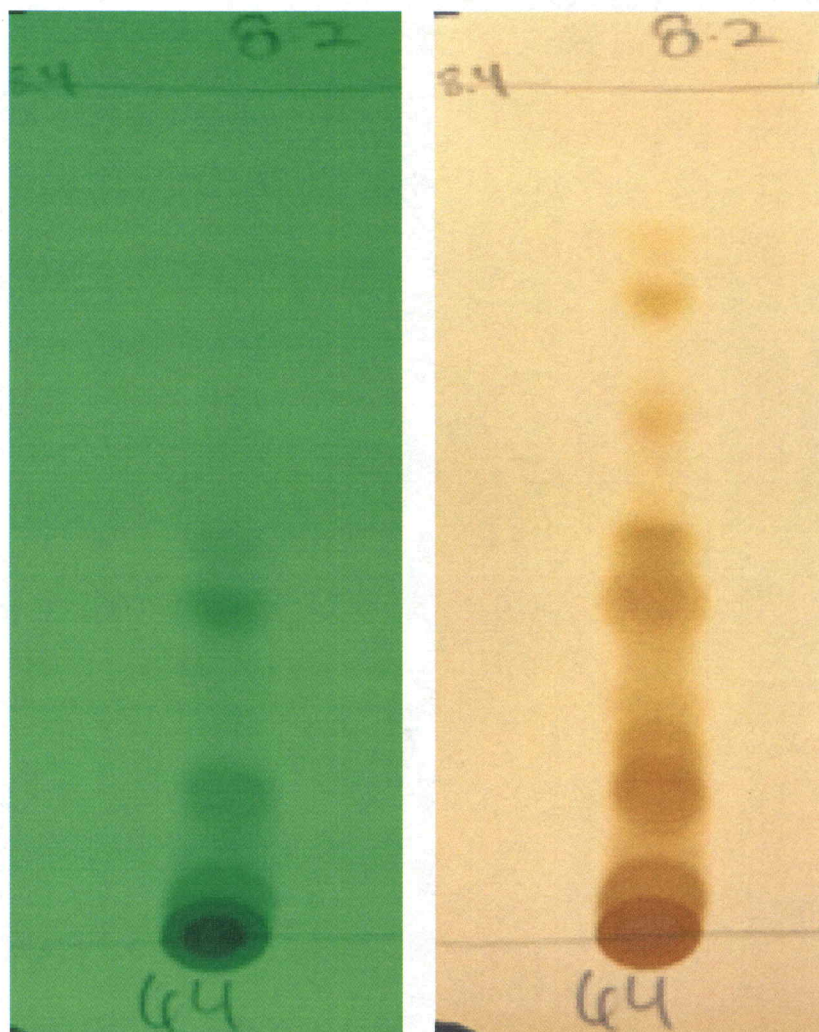


**Figure 9** Visualization of NPPE #11 after separation with 8:2 petroleum ether: ethyl acetate on a silica gel TLC plate. UV light detection is shown on the left, and the 10-minute iodine stain is shown on the right. UV showed four distinct spots, even though one of the spots barely separated from the original. The iodine stain revealed eight distinct spots, with minimal smearing, however most of the spots are overlapped with others. It appears that there could be other spots judging from the iodine stain, however they are faint and hardly discernible.

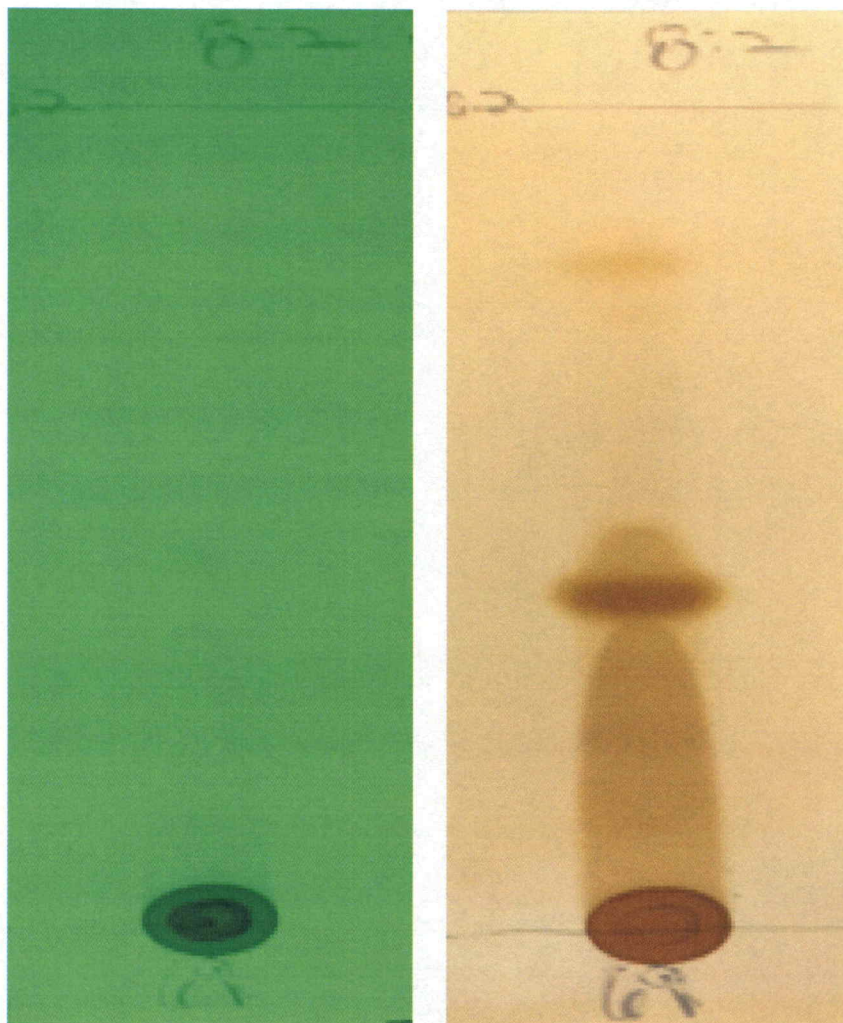


**Figure 10** Visualization of NPPE #13 after separation with 8:2 petroleum ether: ethyl acetate on a silica gel TLC plate. UV light detection is shown on the left, and the 10-minute iodine stain is shown on the right. While UV showed no discernable separation, the iodine stain revealed two distinct spots, accompanied by a decent amount of smearing. It appears that there could be other spots judging from the iodine stain, however they are faint and hardly discernible.



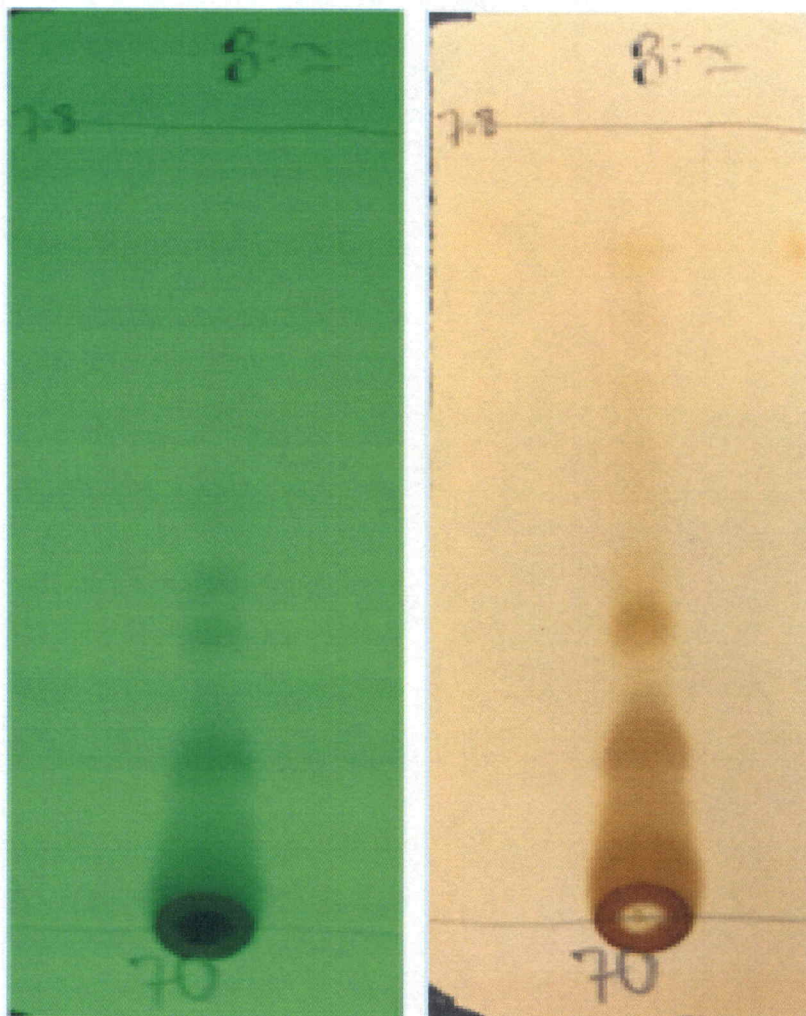


**Figure 11** Visualization of NPPE #14 after separation with 8:2 petroleum ether: ethyl acetate on a silica gel TLC plate. UV light detection is shown on the left, and the 10-minute iodine stain is shown on the right. UV and the iodine stain both showed three distinct spots accompanied by a decent amount of smearing. It appears that there could be other spots, however they are overlapped with other spots, or faint and hardly discernible.

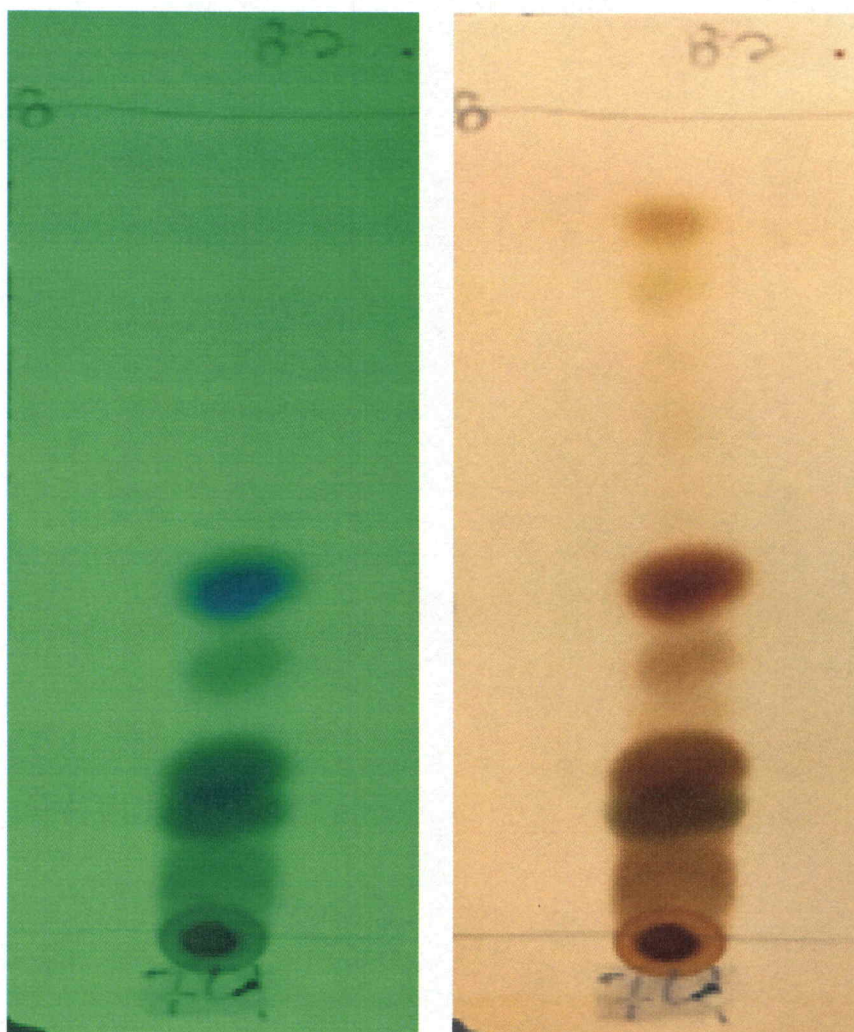


**Figure 12** Visualization of NPPE #16 after separation with 8:2 petroleum ether: ethyl acetate on a silica gel TLC plate. UV light detection is shown on the left, and the 10-minute iodine stain is shown on the right. UV showed five distinct spots, even though one of the spots barely separated from the original. The iodine stain revealed eight distinct spots, with minimal smearing, however half of the spots are overlapped with others. It appears that there could be other spots judging from the colors that appeared after the iodine stain, however they are faint and hardly discernible.

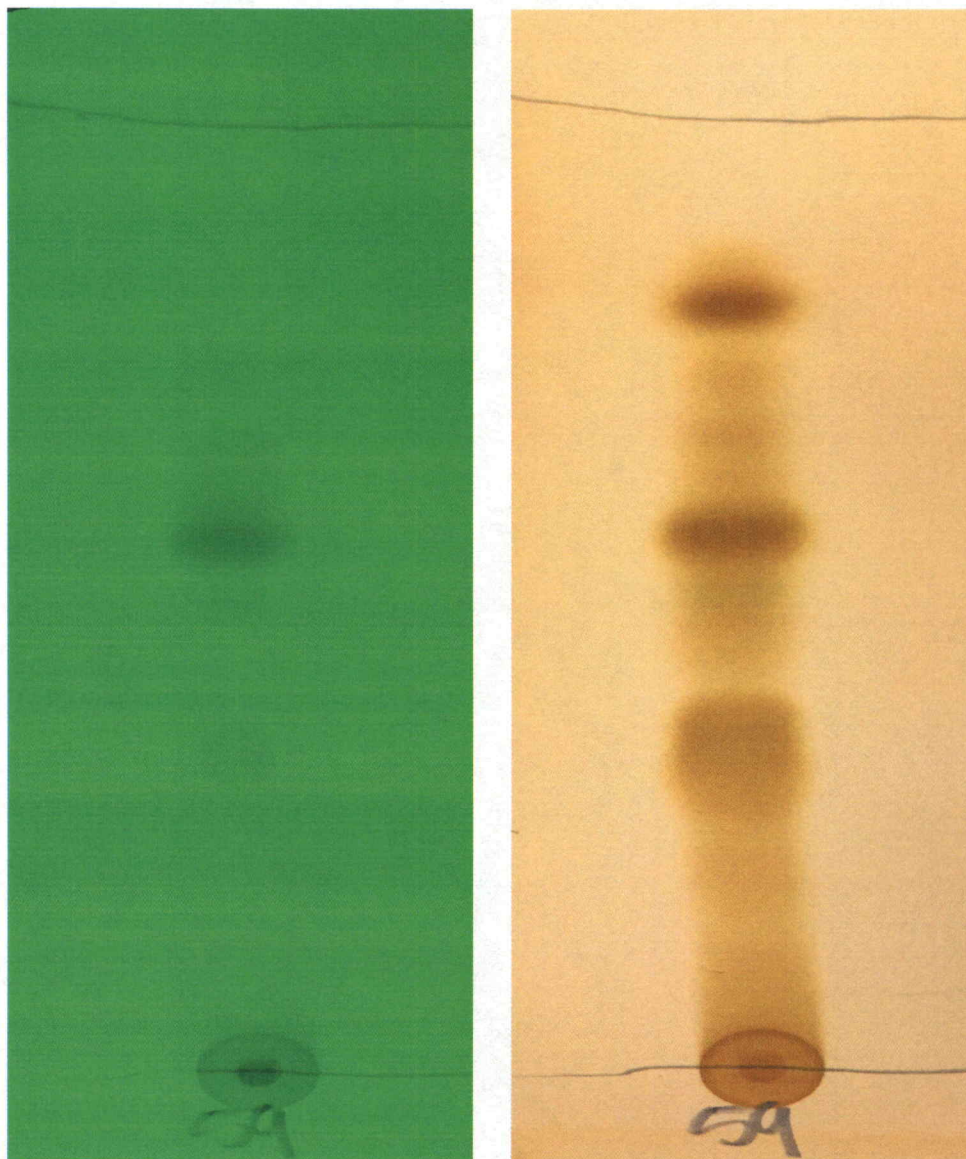


**Figure 13** Visualization of NPPE #7 after separation with 7:3 petroleum ether: ethyl acetate on a silica gel TLC plate. UV light detection is shown on the left, and the 10-minute iodine stain is shown on the right. UV showed three distinct spots, with a few spots that appeared to smear and were not completely separated. The iodine stain also revealed three distinct spots, with slight smearing, although the remaining spots seem overlapped with others.

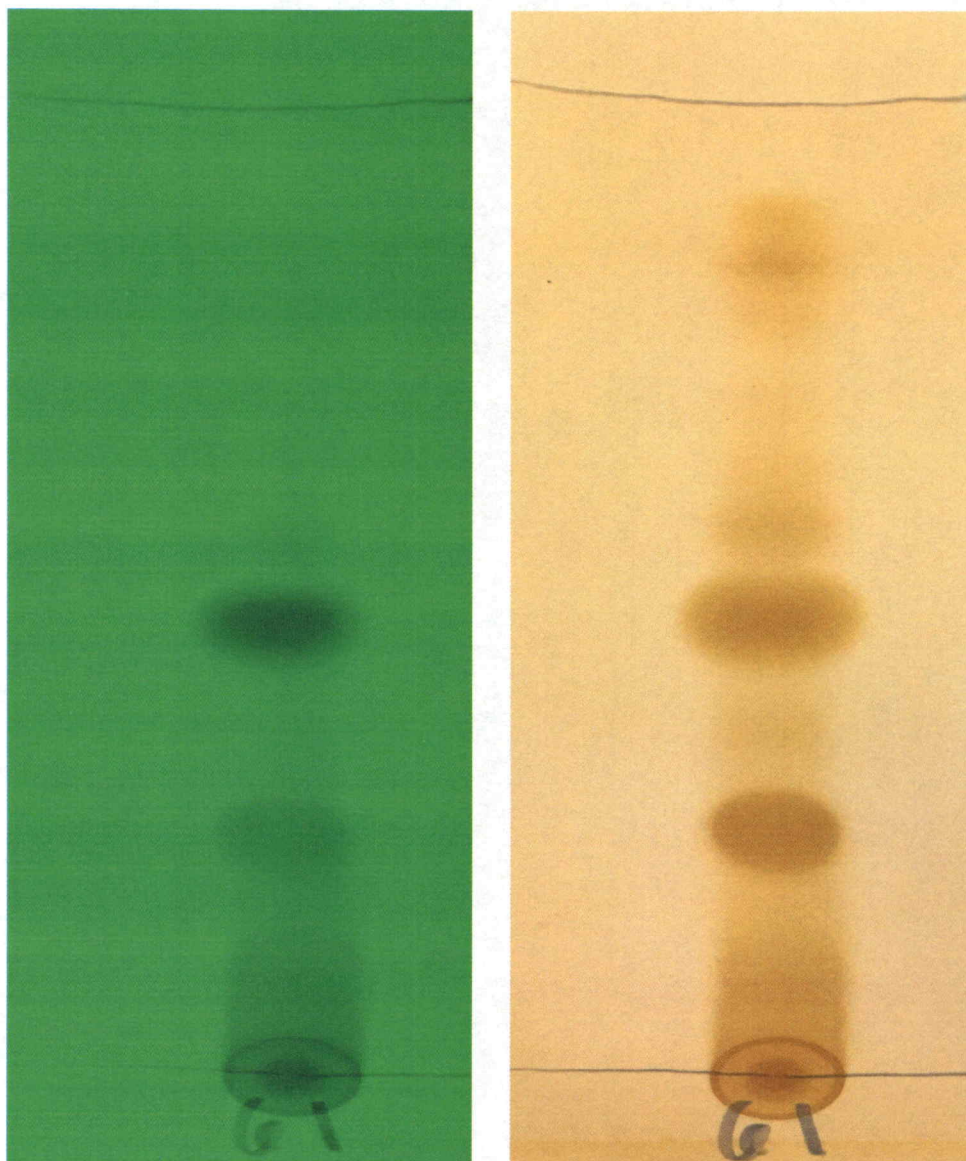


**Figure 14** Visualization of NPPE #9 after separation with 7:3 petroleum ether: ethyl acetate on a silica gel TLC plate. UV light detection is shown on the left, and the 10-minute iodine stain is shown on the right. UV showed three distinct spots, while the iodine stain revealed six distinct spots, with minimal smearing. It appears that there could be other spots judging from the iodine stain, however they are faint and hardly discernible.

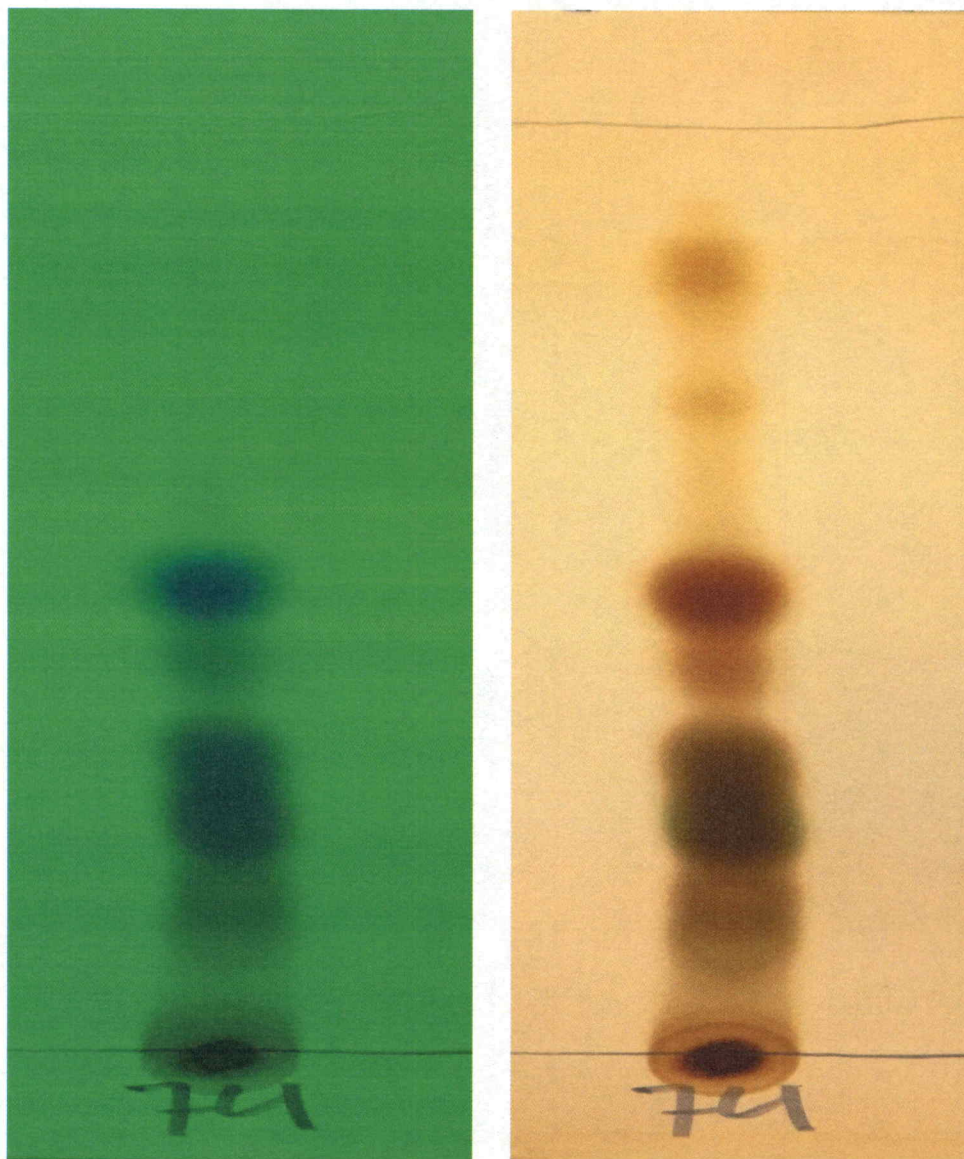


**Figure 15** Visualization of NPPE #16 after separation with 7:3 petroleum ether: ethyl acetate on a silica gel TLC plate. UV light detection is shown on the left, and the 10-minute iodine stain is shown on the right. UV showed six distinct spots, with some of the spots still overlapping. The iodine stain revealed eight distinct spots, with minimal smearing.

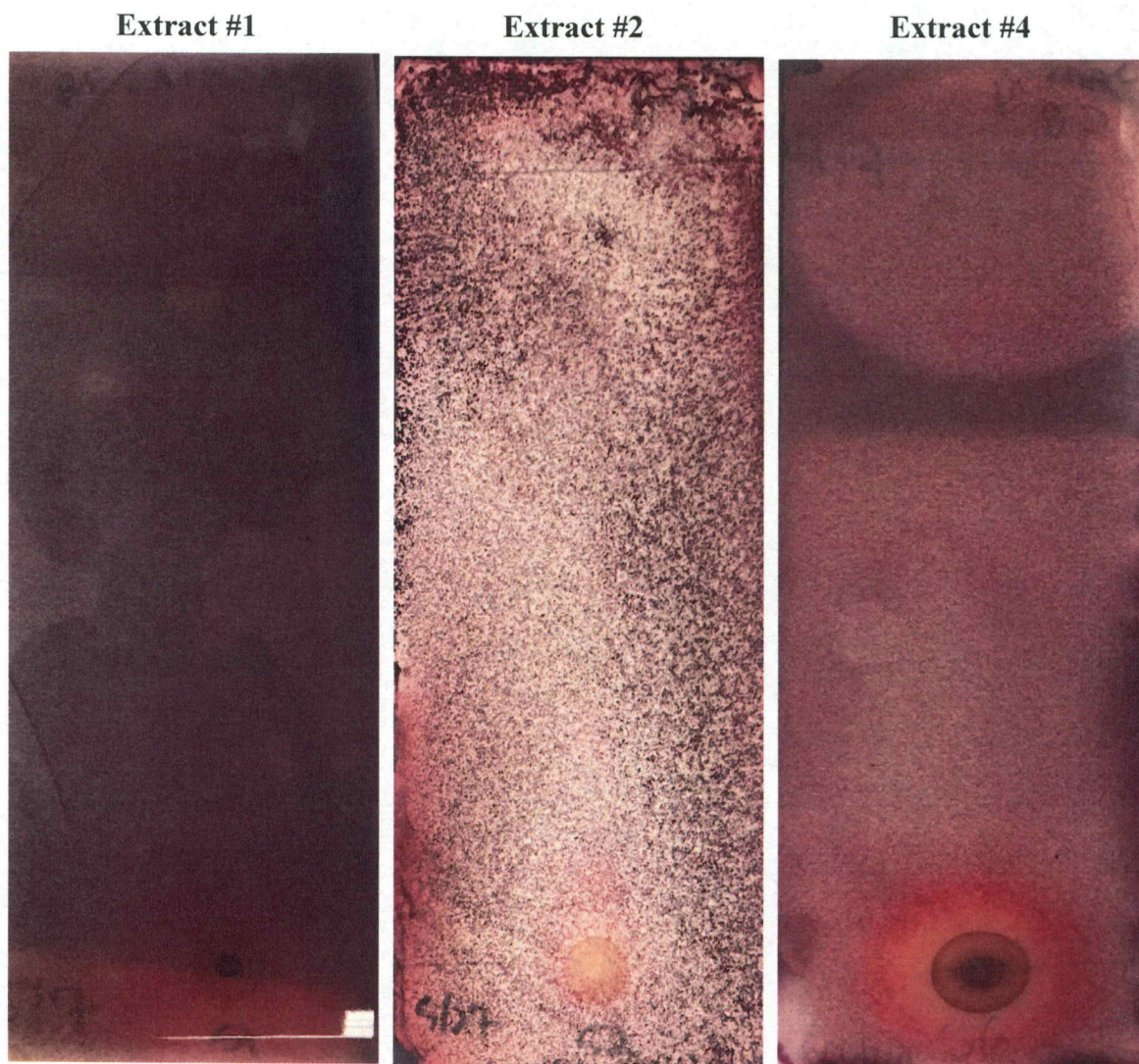


**Figure 16** Images of agar-overlay bioautography for NPPEs #1, #2, and #4 after staining with INT dye for 48 hours. Extract #1 did not provide a zone of inhibition anywhere on the plate. Extracts #2 and #4 did not provide a zone of inhibition after separation, however the appearance of an inhibition zone can be seen over the original spot, suggesting that the active anticryptococcal component(s) were not separated with the solvent system PetEt:EtOAc in a ratio of 8:2.

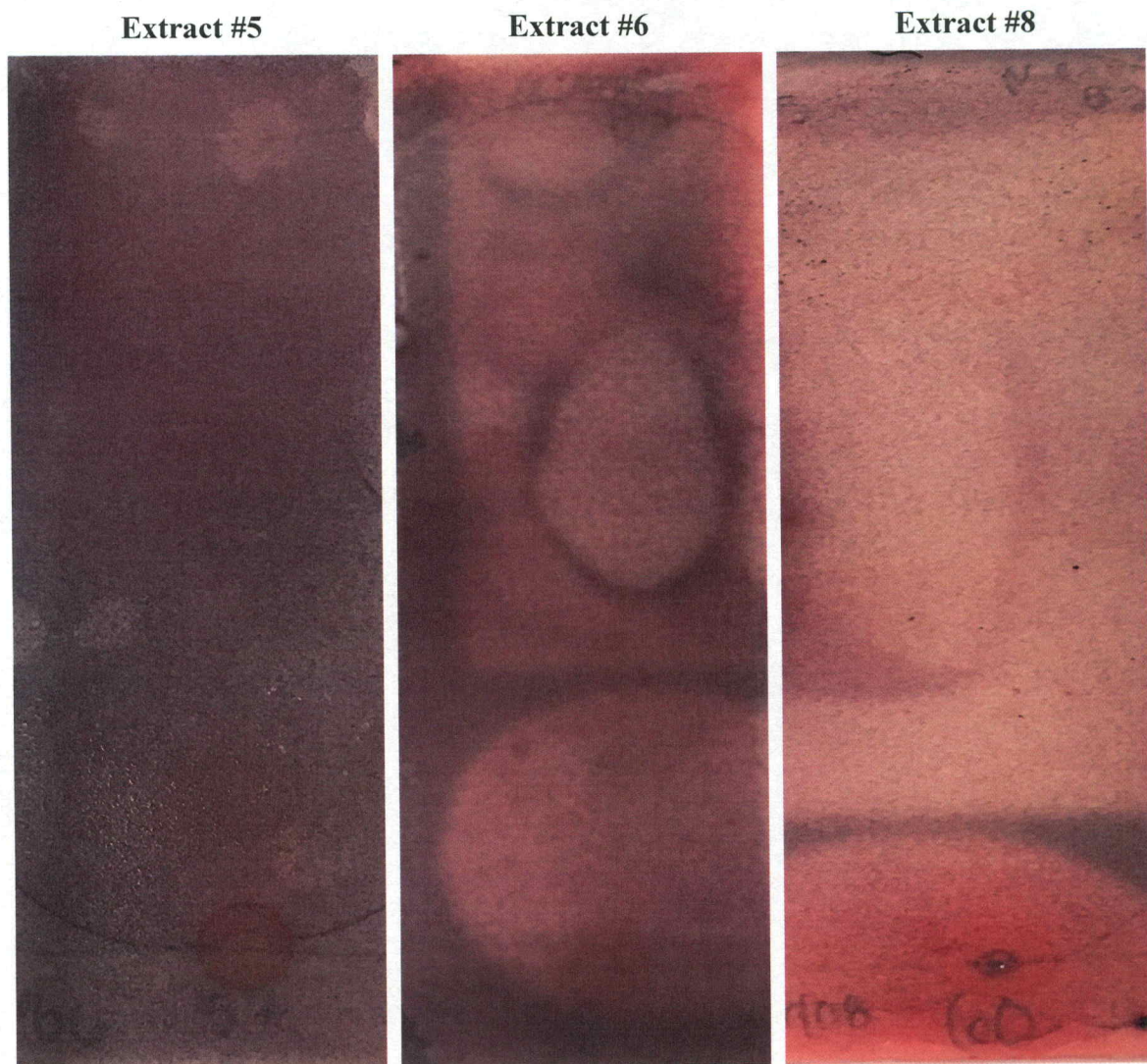


**Figure 17** Images of agar-overlay bioautography for NPPEs #5, #6 and #8 after staining with INT dye for 48 hours. All three extracts did not provide a zone of inhibition after separation, suggesting that the active anticryptococcal component(s) were not separated with the solvent system PetEt:EtOAc in a ratio of 8:2.

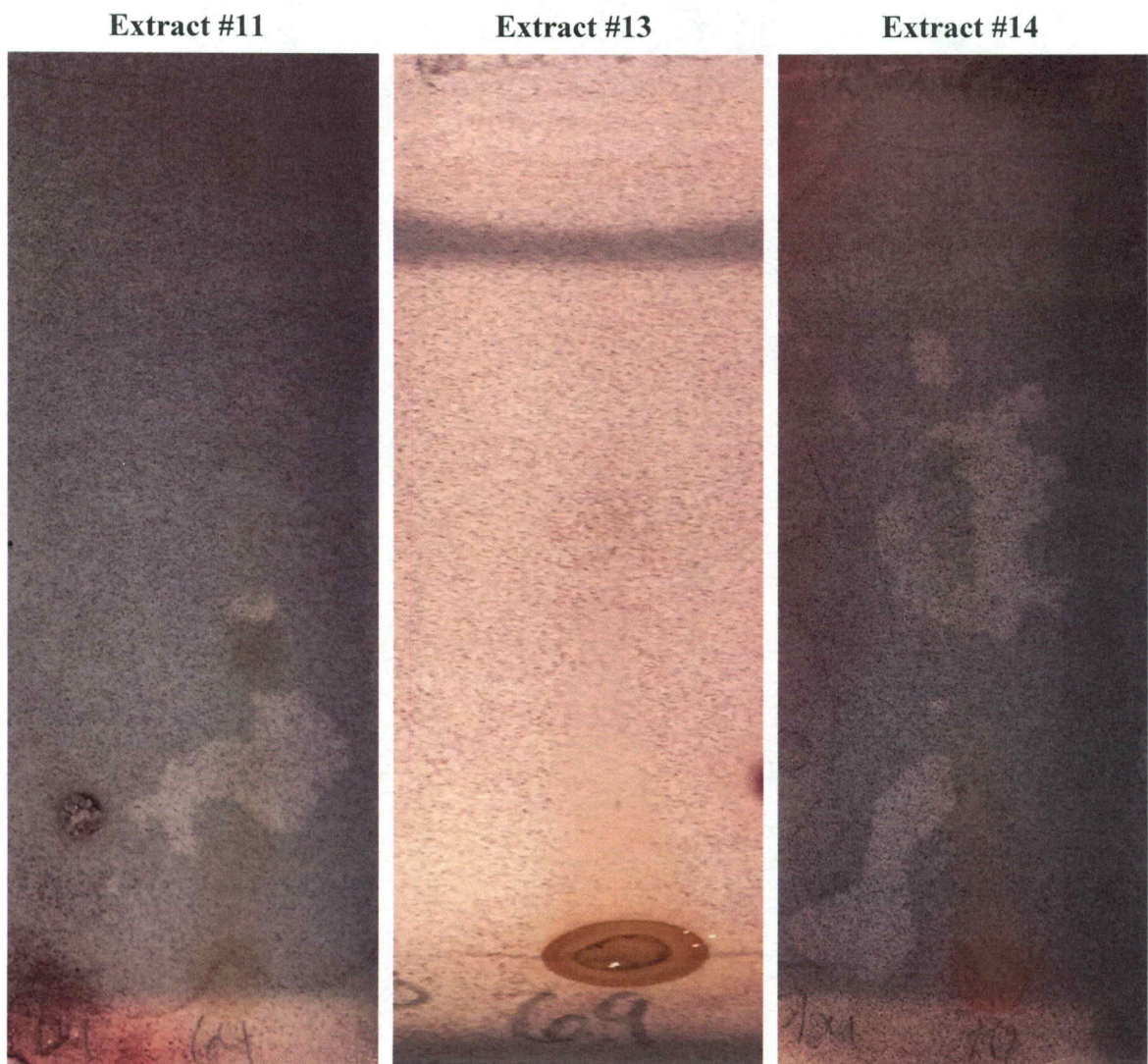


**Figure 18** Images of agar-overlay bioautography for NPPEs #11, #13, and #14 after staining with INT dye for 48 hours. Extracts #11 and #14 did not provide any zones of inhibition, however an inhibition zone can be seen over the original spot of extract #13, suggesting that the active anticryptococcal component(s) were not separated with the solvent system PetEt:EtOAc in a ratio of 8:2.



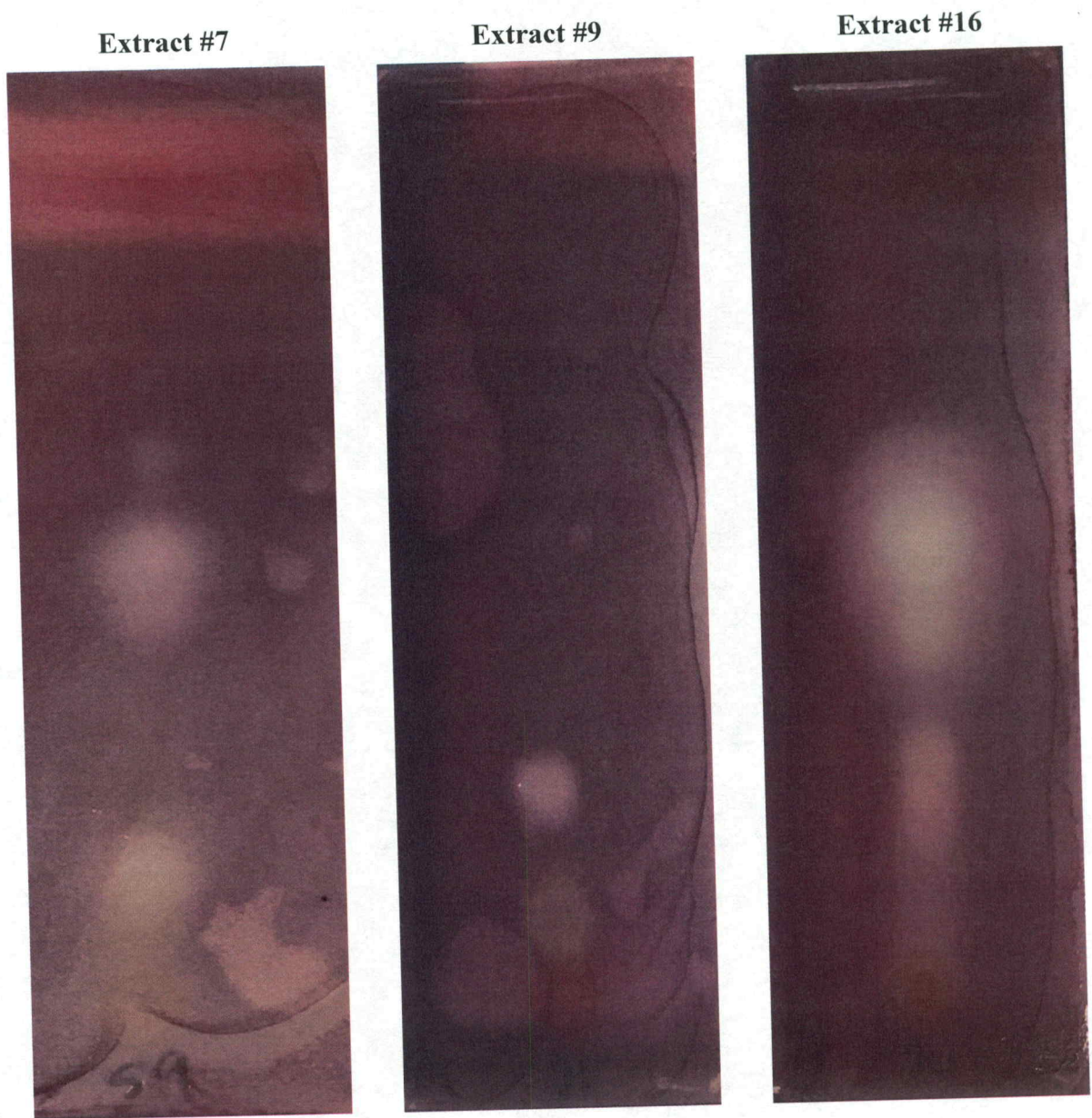


**Figure 19** Images of agar-overlay bioautography for NPPEs #7, #9, and #16 after staining with INT dye for 48 hours. The appearance of obvious inhibition zones after separation suggests that the components are in high enough concentration to inhibit fungal growth.

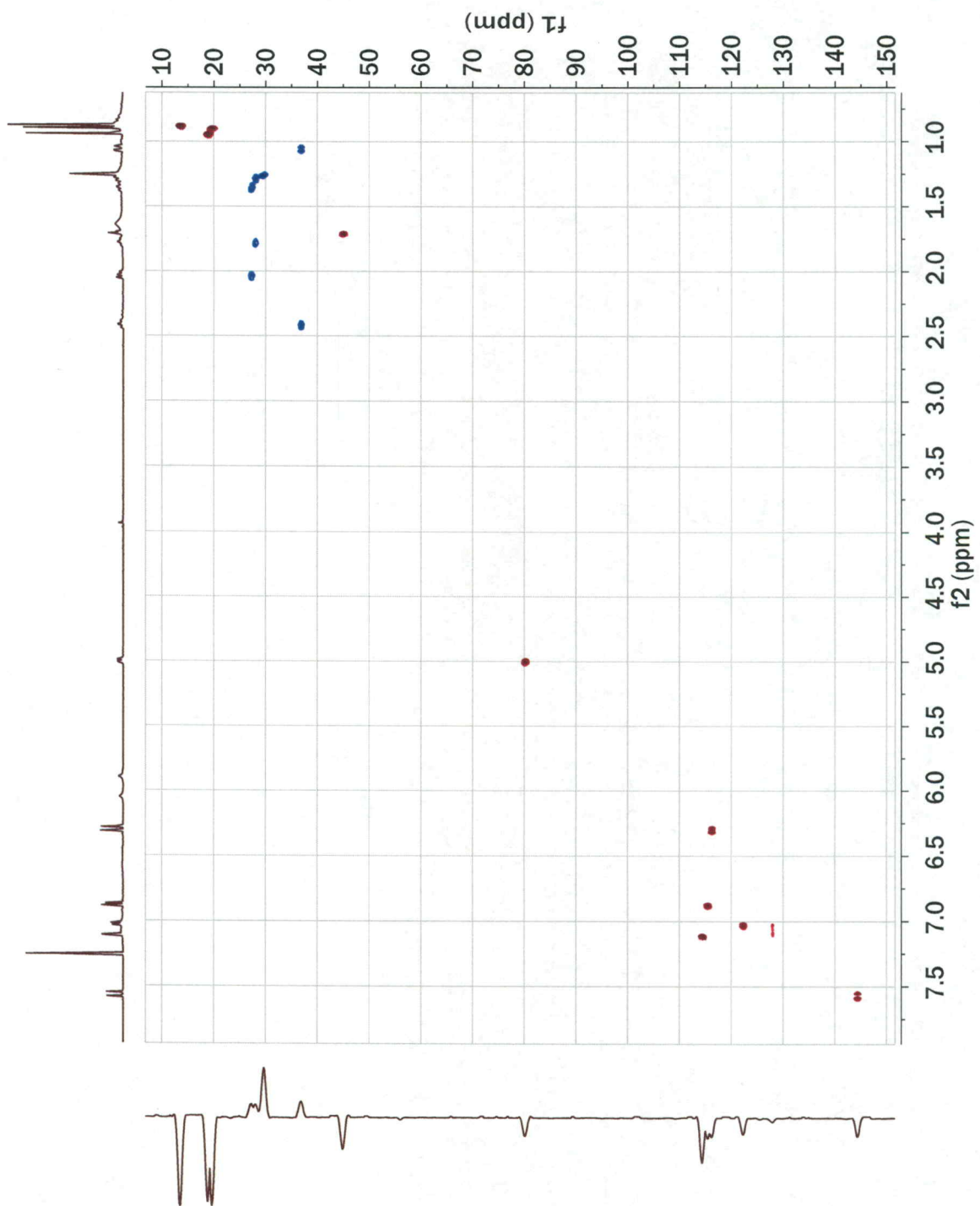


**Figure 20** Heteronuclear single quantum correlation (HSQC) spectrum of prep-TLC isolate #3 (NPPE #9,  $R_f = 0.25$ ). Spectrum was collected on a 500 MHz Varian Unity Inova spectrometer. Carbon sweep width was 25141 Hz centered at 90 ppm while hydrogen sweep width was 5006 Hz centered at 5.5 ppm. Number of increments was 128 while number of transient scans per t1 increments was 4. NUS with 37.5% sampling density and 256 increments in reconstituted data was used.

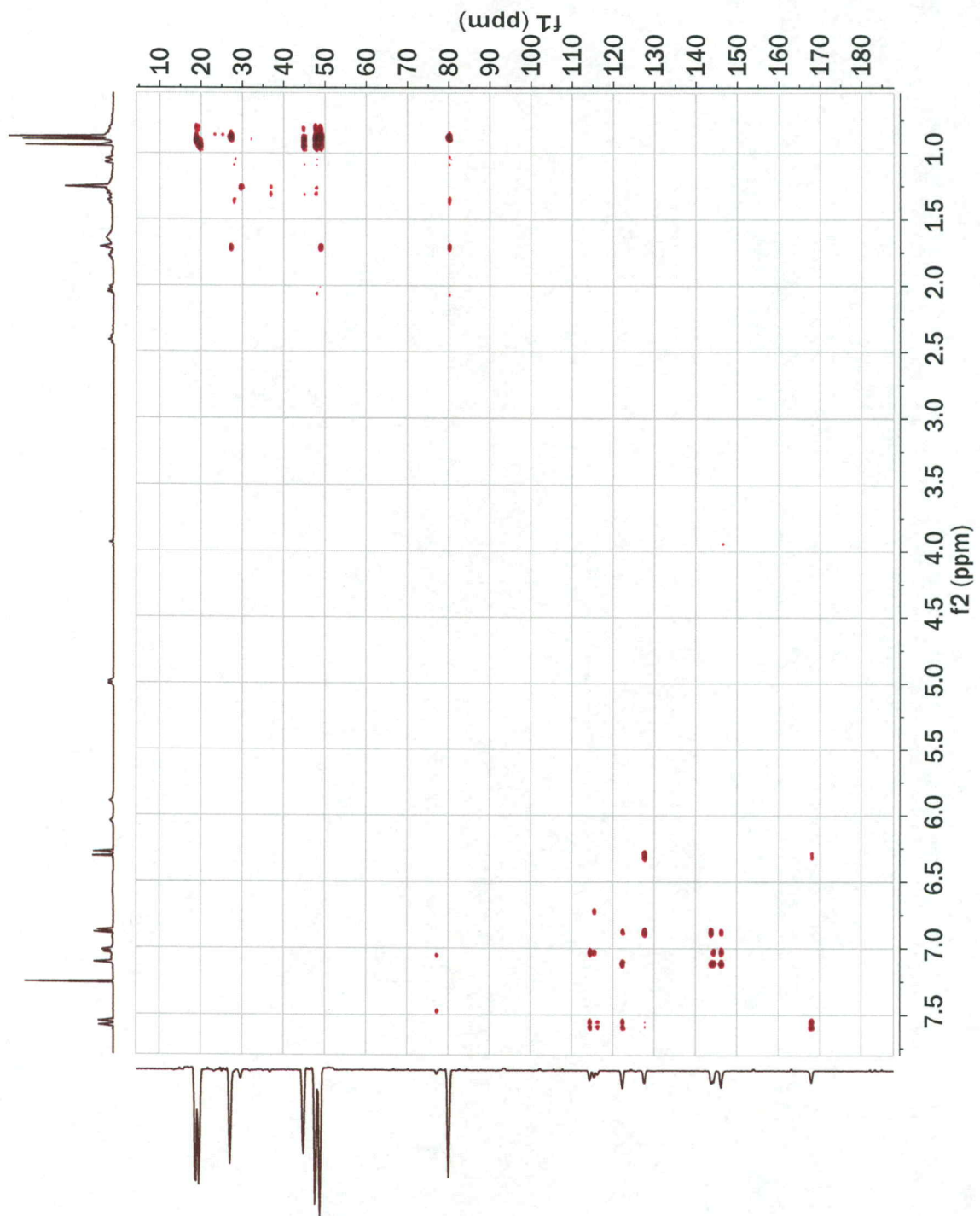


**Figure 21** Heteronuclear multiple bond correlation (HMBC) spectrum of prep-TLC isolate #3 (NPPE #9,  $R_f = 0.25$ ). Spectrum was collected on a 500 MHz Varian Unity Inova spectrometer. Carbon sweep width was 30166 Hz centered at 105 ppm while hydrogen sweep width was 5006 Hz centered at 5.5 ppm. Number of increments was 256 while number of transient scans per t1 increments was 4. NUS with 50.0% sampling density and 512 increments in reconstituted data was used.

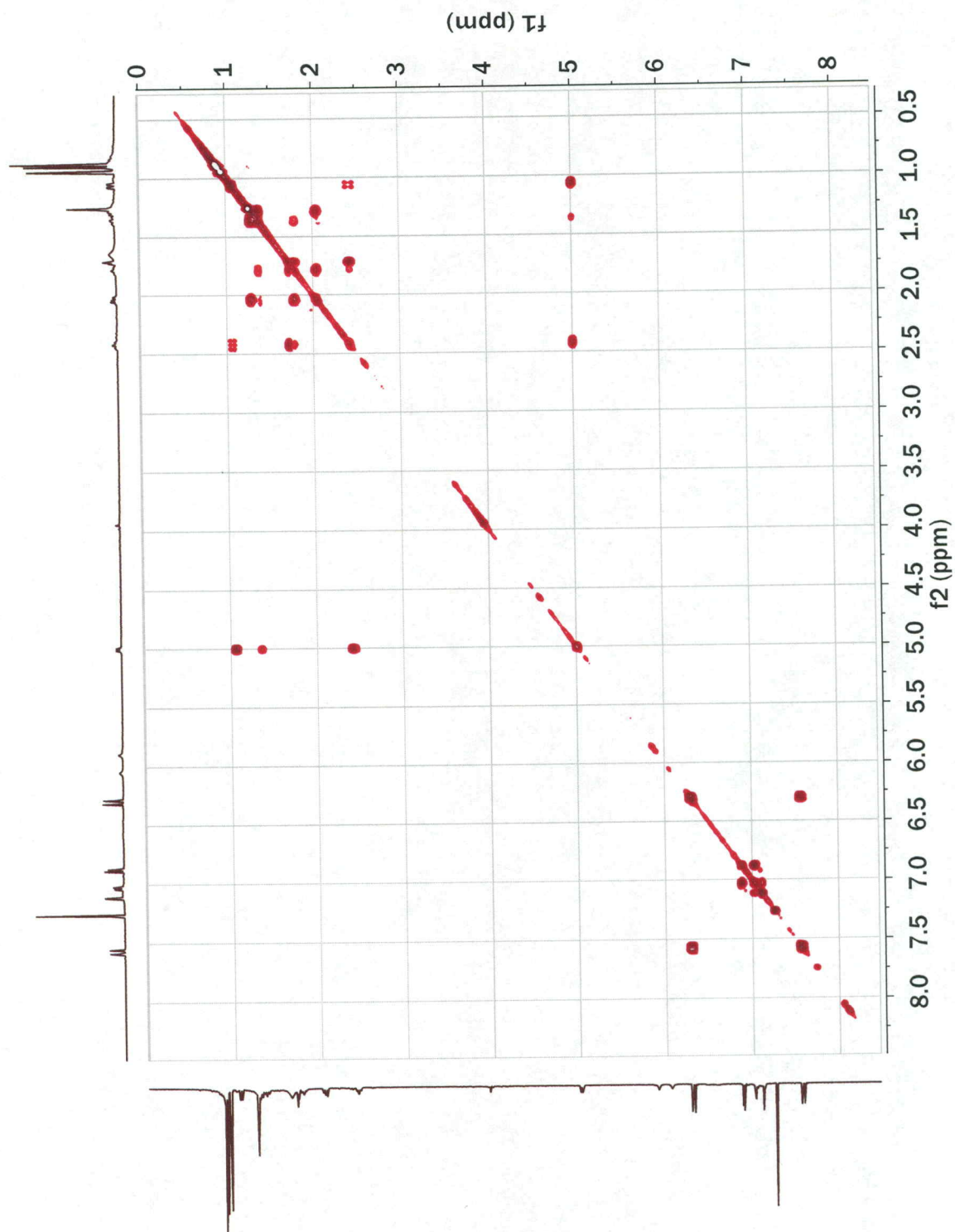


**Figure 22**  $^1\text{H}$ - $^1\text{H}$  correlation (COSY) spectrum of prep-TLC isolate #3 (NPPE #9,  $R_f = 0.25$ ). Spectrum was collected on a 500 MHz Varian Unity Inova spectrometer. Hydrogen sweep width was 5006 Hz centered at 5.5 ppm. Number of increments was 512 while number of transient scans per t1 increments was 2. NUS with 50.0% sampling density and 512 increments in reconstituted data was used.

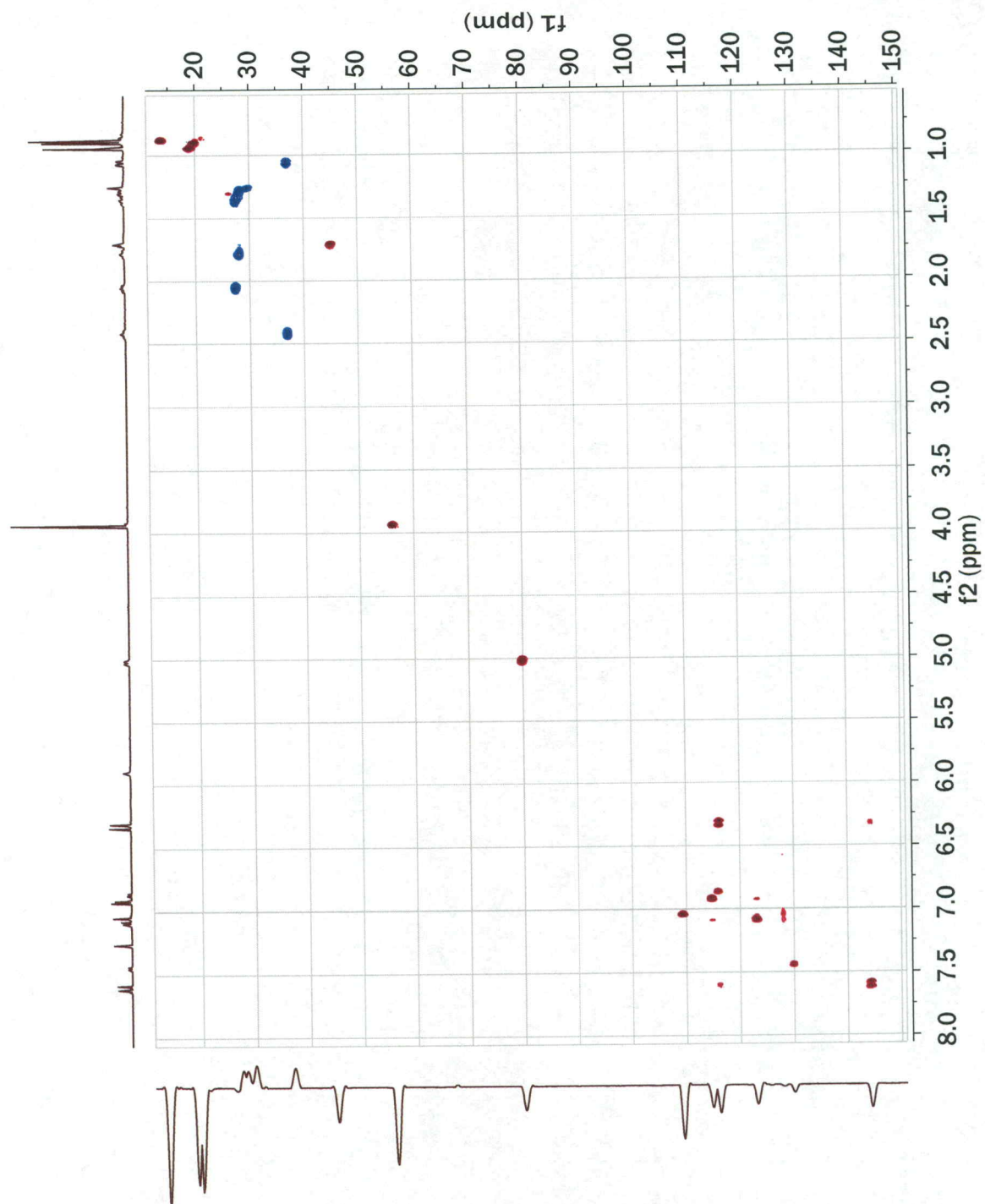


**Figure 23** Heteronuclear single quantum correlation (HSQC) spectrum of prep-TLC isolate #4 (NPPE #9,  $R_f = 0.51$ ). Spectrum was collected on a 500 MHz Varian Unity Inova spectrometer. Carbon sweep width was 25141 Hz centered at 90 ppm while hydrogen sweep width was 5006 Hz centered at 5.5 ppm. Number of increments was 128 while number of transient scans per t1 increments was 4. NUS with 37.5% sampling density and 256 increments in reconstituted data was used.

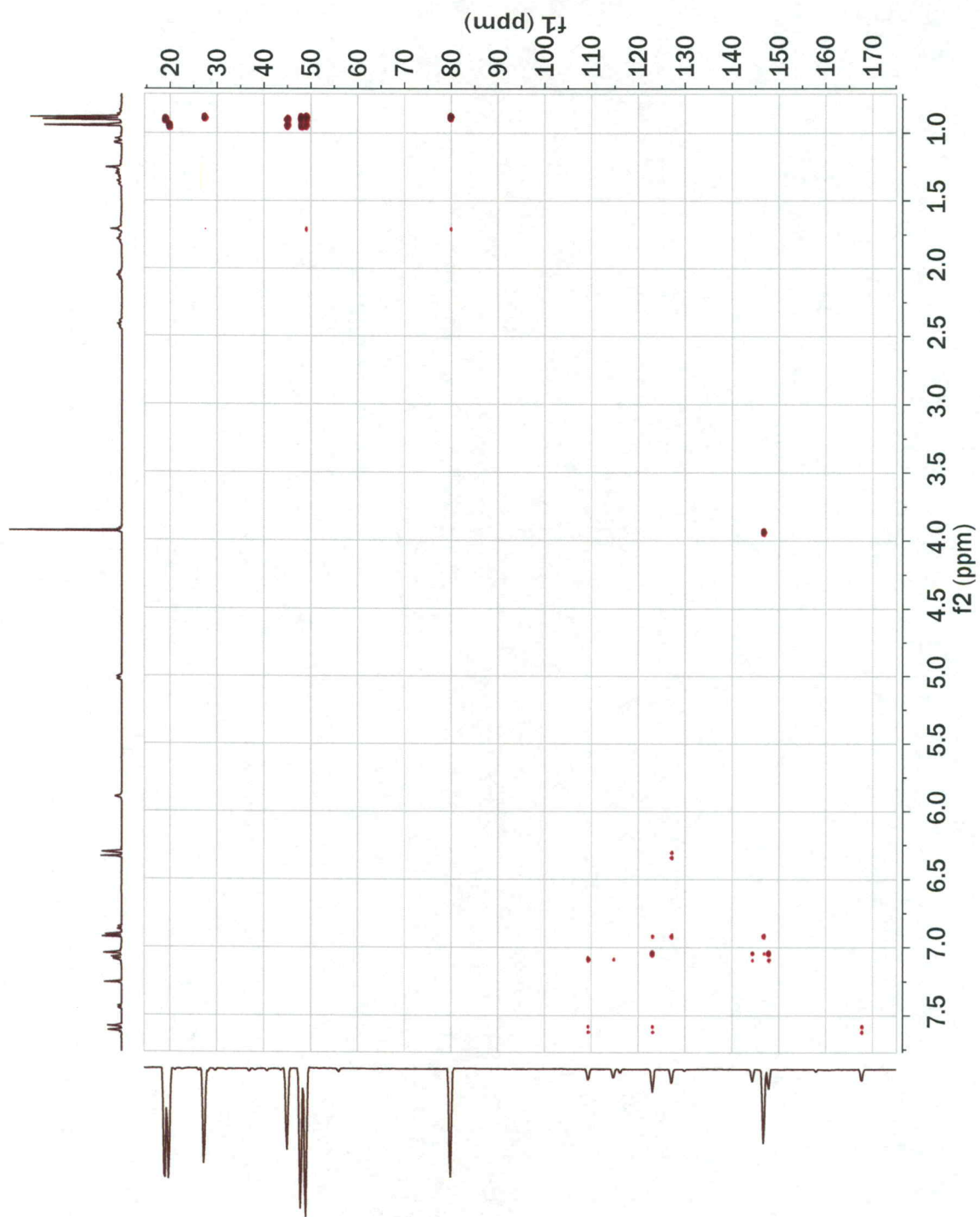


**Figure 24** Heteronuclear multiple bond correlation (HMBC) spectrum of prep-TLC isolate #4 (NPPE #9,  $R_f = 0.51$ ). Spectrum was collected on a 500 MHz Varian Unity Inova spectrometer. Carbon sweep width was 30166 Hz centered at 105 ppm while hydrogen sweep width was 5006 Hz centered at 5.5 ppm. Number of increments was 256 while number of transient scans per t1 increments was 4. NUS with 50.0% sampling density and 512 increments in reconstituted data was used.

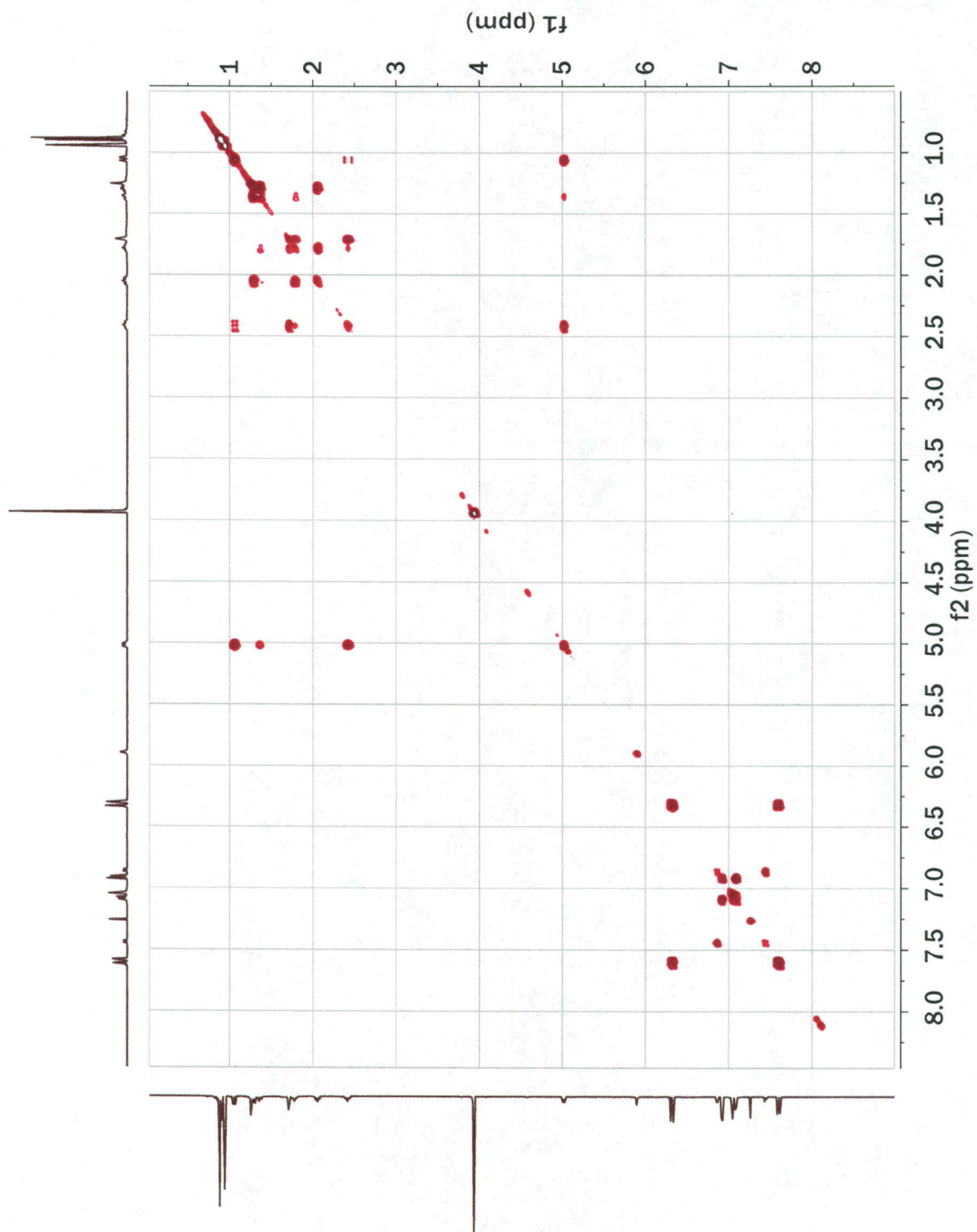


**Figure 25**  $^1\text{H}$ - $^1\text{H}$  correlation (COSY) spectrum of prep-TLC isolate #4 (NPPE #9,  $R_f = 0.51$ ). Spectrum was collected on a 500 MHz Varian Unity Inova spectrometer. Hydrogen sweep width was 5006 Hz centered at 5.5 ppm. Number of increments was 512 while number of transient scans per t1 increments was 2. NUS with 50.0% sampling density and 512 increments in reconstituted data was used.

## REFERENCES

- Abad, Maria José. 2006. "Active Antifungal Substances from Natural Sources." *Arkivoc* 2007 (vii):116–45.
- Amiguet, Virginie Treyvaud, Philippe Petit, Chieu Anh Ta, Ronaldo Nuñez, Pablo Sánchez-Vindas, Luis Poveda Alvarez, Myron L. Smith, John Thor Arnason, and Tony Durst. 2006. "Phytochemistry and Antifungal Properties of the Newly Discovered Tree *Pleodendron Costaricense*." *Journal of Natural Products* 69 (7):1005–9.
- Balouiri, Mounyr, Moulay Sadiki, and Saad Koraichi Ibsouda. 2016. "Methods for in Vitro Evaluating Antimicrobial Activity: A Review." *Journal of Pharmaceutical Analysis* 6 (2). Elsevier:71–79.
- Brown, G. D., D. W. Denning, N. A. R. Gow, S. M. Levitz, M. G. Netea, and T. C. White. 2012. "Hidden Killers: Human Fungal Infections." *Science Translational Medicine* 4 (165):165rv13-165rv13.
- Campoy, Sonia, and José L. Adrio. 2017. "Antifungals." *Biochemical Pharmacology* 133:86–96.
- Demain, Arnold L. 2014. "Importance of Microbial Natural Products and the Need to Revitalize Their Discovery." *Journal of Industrial Microbiology and Biotechnology* 41 (2):185–201.
- DeMera, Jason H., and Esther R. Angert. 2004. "Comparison of the Antimicrobial Activity of Honey Produced by *Tetragonisca Angustula* (Meliponinae) and *Apis Mellifera* from Different Phytogeographic Regions of Costa Rica." *Apidologie* 35 (4):411–17.



- Desjardins, Christopher, Charles Giamberardino, Sean Sykes, Chen-Hsin Yu, Jennifer Tenor, Yuan Chen, Timothy Yang, Alexander Jones, Sheng Sun, and Miriam Haverkamp. 2017. "Population Genomics And The Evolution Of Virulence In The Fungal Pathogen *Cryptococcus Neoformans*." *Genome Research* 27 (7):1207–19.
- Deskins, Caitlin E, Bernhard Vogler, Noura S Dosoky, Bhuwan K Chhetria, William A Haber, and William N Setzer. 2014. "Phytochemical Investigations of *Lonchocarpus* Bark Extracts from Monteverde, Costa Rica." *Natural Product Communications* 9 (4):507–10.
- Dewanjee, Saikat, Moumita Gangopadhyay, Niloy Bhattacharya, Ritu Khanra, and Tarun K. Dua. 2015. "Bioautography and Its Scope in the Field of Natural Product Chemistry." *Journal of Pharmaceutical Analysis* 5 (2). Elsevier:75–84.
- Domaneschi, Carina, Pedro Henrique Magalhães Cardoso, Débora Moreira, Marcia de Souza Carvalho Melhem, Luciana da Silva Ruiz, Diniz Pereira Leite Júnior, Eriques Gonçalves da Silva, et al. 2018. "Characterization of Clinical and Environmental Isolates of *Cryptococcus neoformans*/*Cryptococcus gattii* Complex Maintained in Yeast Culture Collection in São Paulo, Brazil." *Open Journal of Epidemiology* 08 (02):76–92.
- Eason, Hannah M, and William N Setzer. 2007. "Bark Essential Oil Composition of *Cedrela Tonduzii* C. DC.(Meliaceae) from Monteverde, Costa Rica." *Records of Natural Products* 1 (2–3):24–27.
- Fabri, Rodrigo Luiz, Mauro Silva Nogueira, Jussara dos Reis Moreira, Maria Lúcia Morcef Bouzada, and Elita Scio. 2011. "Identification of Antioxidant and Antimicrobial Compounds of *Lippia* Species by Bioautography." *Journal of Medicinal Food* 14 (7–8):840–46.
- Favre-Godal, Quentin, Emerson Ferreira Queiroz, and Jean Luc Wolfender. 2013. "Latest Developments in Assessing Antifungal Activity Using TLC-Bioautography: A Review." *Journal of AOAC International* 96 (6):1175–88.
- Fernández, Lucía R., Estefanía Butassi, Laura Svetaz, Susana A. Zacchino, Jorge A. Palermo, and Marianela Sánchez. 2014. "Antifungal Terpenoids from *Hyalis Argentea* Var. *Latisquama*." *Journal of Natural Products* 77 (7):1579–85.

- Ficker, C E, J T Arnason, P S Vindas, L P Alvarez, K Akpagana, M Gbeassor, C De Souza, and M L Smith. 2003. "Inhibition of Human Pathogenic Fungi by Ethnobotanically Selected Plant Extracts." *Mycoses* 46 (1–2):29–37.
- Guerrini, Alessandra, Gianni Sacchetti, Alessandro Grandini, Antonella Spagnoletti, Mercedes Asanza, and Laura Scalvenzi. 2016. "Cytotoxic Effect and TLC Bioautography-Guided Approach to Detect Health Properties of Amazonian *Hedyosmum Sprucei* Essential Oil." *Evidence-Based Complementary and Alternative Medicine* 2016.
- Gurnani, N, D Mehta, M Gupta, and B K Mehta. 2014. "Natural Products : Source of Potential Drugs." *African Journal of Basic & Applied Sciences* 6 (6):171–86.
- Hardison, Sarah E., and Gordon D. Brown. 2012. "C-Type Lectin Receptors Orchestrate Antifungal Immunity." *Nature Immunology* 13 (9):817–22.
- Jung, Eric H, David J Meyers, Jürgen Bosch, and Arturo Casadevall. 2018. "Novel Antifungal Compounds Discovered in Medicines for Malaria Venture's Malaria Box." *MSphere* 3 (2):e00537-17.
- Madeira-Lopes, A., M. Teresa Plácido, and C. Cabeça-Silva. 1986. "Comparative Study of the Temperature Profiles of Growth and Death of the Pathogenic Yeast *Cryptococcus Neoformans* and the Non-Pathogenic *Cryptococcus Albidus*." *Journal of Basic Microbiology* 26 (1):43–47.
- Marston, A. 2011. "Thin-Layer Chromatography with Biological Detection in Phytochemistry." *Journal of Chromatography A* 1218 (19). Elsevier B.V.:2676–83.
- Montagna, Maria Teresa, Antonella De Donno, Giuseppina Caggiano, Francesca Serio, Osvalda De Giglio, Francesco Bagordo, R. D'Amicis, Shawn R. Lockhart, and Massimo Cogliati. 2018. "Molecular Characterization of *Cryptococcus Neoformans* and *Cryptococcus Gattii* from Environmental Sources and Genetic Comparison with Clinical Isolates in Apulia, Italy." *Environmental Research* 160 (June 2017). Elsevier Inc.:347–52.
- Newman, David J., and Gordon M. Cragg. 2016. "Natural Products as Sources of New Drugs from 1981 to 2014." *Journal of Natural Products* 79 (3):629–61.

- Ogungbe, Ifedayo V, Rebecca A Crouch, William A Haber, and William N Setzer. 2010. "Phytochemical Investigation of *Verbesina Turbacensis* Kunth: Trypanosome Cysteine Protease Inhibition by (-)-Bornyl Esters." *Natural Product Communications* 5 (8):1161–66.
- Park, Benjamin J, Kathleen A Wannemuehler, Barbara J Marston, Nelesh Govender, Peter G Pappas, and Tom M Chiller. 2009. "Estimation of the Current Global Burden of Cryptococcal Meningitis among Persons Living with HIV/AIDS." *Aids* 23 (4):525–30.
- Perfect, John R. 2017. "The Antifungal Pipeline: A Reality Check." *Nature Reviews Drug Discovery* 16 (9):603–16.
- Perfect, John R., and Gary M. Cox. 1999. "Drug Resistance in *Cryptococcus Neoformans*." *Drug Resistance Updates : Reviews and Commentaries in Antimicrobial and Anticancer Chemotherapy* 2 (4):259–69.
- Perlin, David S., Riina Rautemaa-Richardson, and Ana Alastruey-Izquierdo. 2017. "The Global Problem of Antifungal Resistance: Prevalence, Mechanisms, and Management." *The Lancet Infectious Diseases* 17 (12). Elsevier Ltd:e383–92.
- Polvi, Elizabeth J., Xinliu Li, Teresa R. O'Meara, Michelle D. Leach, and Leah E. Cowen. 2015. "Opportunistic Yeast Pathogens: Reservoirs, Virulence Mechanisms, and Therapeutic Strategies." *Cellular and Molecular Life Sciences* 72 (12). Springer Basel:2261–87.
- Prieto, Juliet a, Oscar J Patiño, Wilman a Delgado, Jenny P Moreno, and Luis E Cuca. 2011. "Chemical Composition, Insecticidal, and Antifungal Activities of Fruit Essential Oils of Three Colombian *Zanthoxylum* Species." *Chilean Journal Of Agriculture Research* 71 (March):73–82.
- Rajasingham, Radha, Rachel M. Smith, Benjamin J. Park, Joseph N. Jarvis, Nelesh P. Govender, Tom M. Chiller, David W. Denning, Angela Loyse, and David R. Boulware. 2017. "Global Burden of Disease of HIV-Associated Cryptococcal Meningitis: An Updated Analysis." *The Lancet Infectious Diseases* 17 (8). Elsevier Ltd:873–81.

- Revie, Nicole M., Kali R. Iyer, Nicole Robbins, and Leah E. Cowen. 2018. "Antifungal Drug Resistance: Evolution, Mechanisms and Impact." *Current Opinion in Microbiology* 45 (Figure 2). Elsevier Ltd:70–76.
- Setzer, Mary C, Debra M Moriarity, Robert O Lawton, William N Setzer, Glenn A Gentry, and William A Haber. 2003. "Phytomedicinal Potential of Tropical Cloudforest Plants from Monteverde, Costa Rica." *Revista de Biología Tropical* 51 (3–4).
- Setzer, William N. 2006. "Chemical Compositions of the Bark Essential Oils of *Croton Monteverdensis* and *Croton Niveus* from Monteverde, Costa Rica." *Natural Product Communications* 1 (7):567–72.
- Setzer, William N, Bernhard Vogler, Jennifer M Schmidt, Julie L Petty, and William A Haber. 2005. "Isolation of Cupanoside, a Novel Cytotoxic and Antibacterial Long-Chain Fatty Alcohol Glycoside from the Bark of *Cupania Glabra*." *Plant Medica* 71 (7):686–88.
- Smith, Tyler, Kimberly Kawa, Veronica Eckl, Claire Morton, and Ryan Stredney. 2017. "Herbal Supplement Sales in US Increase 7.7 % in 2016." *The Journal of the American Botanical Council*, no. 115:56–65.
- Surapuram, Venkatasachaitanya, William N Setzer, Robert L McFeeters, and Hana McFeeters. 2014. "Antifungal Activity of Plant Extracts against *Aspergillus Niger* and *Rhizopus Stolonifer*." *Natural Product Communications* 9 (11):1603–5.
- Svetaz, Laura, Federico Zuljan, Marcos Derita, Elisa Petenatti, Giselle Tamayo, Armando Cáceres, Valdir Cechinel Filho, et al. 2010. "Value of the Ethnomedical Information for the Discovery of Plants with Antifungal Properties. A Survey among Seven Latin American Countries." *Journal of Ethnopharmacology* 127 (1):137–58.
- Tavares, De Luciana C., Graciane Zanon, Andréia D. Weber, Alexandre T. Neto, Clarice P. Mostardeiro, Ivana B.M. Da Cruz, Raul M. Oliveira, Vinicius Ilha, Ionara I. Dalcol, and Ademir F. Morel. 2014. "Structure-Activity Relationship of Benzophenanthridine Alkaloids from *Zanthoxylum Rhoifolium* Having Antimicrobial Activity." *PLoS ONE* 9 (5).
- Xie, J L, E J Polvi, T Shekhar-Guturja, and L E Cowen. 2014. "Elucidating Drug Resistance in Human Fungal Pathogens." *Future Microbiology* 9 (4):523–42.